# INTERPLAY OF STRESS RELEASE RANGE AND DISORDER IN FRACTURE

*By*

**SUBHADEEP ROY**

**PHYS10201005003**

**The Institute of Mathematical Sciences, Chennai**

***A thesis submitted to the***

***Board of Studies in Mathematical Sciences***

***In partial fulfillment of requirements***

***for the Degree of***

**DOCTOR OF PHILOSOPHY**

***of***

**HOMI BHABHA NATIONAL INSTITUTE**

**July, 2016**

# Homi Bhabha National Institute

## Recommendations of the Viva Voce Committee

As members of the Viva Voce Committee, we certify that we have read the dissertation prepared by Subhadeep Roy entitled "Interplay of stress release range and disorder in fracture" and recommend that it may be accepted as fulfilling the thesis requirement for the award of Degree of Doctor of Philosophy.

_____ Date:

Guide - Purusattam Ray

_____ Date:

Examiner -

_____ Date:

Member 1 - R. Shankar

_____ Date:

Member 2 - R. Rajesh

_____ Date:

Member 3 - Ronojoy Adhikari

Final approval and acceptance of this thesis is contingent upon the candidate's submission of the final copies of the thesis to HBNI.

I hereby certify that I have read this thesis prepared under my direction and recommend that it may be accepted as fulfilling the thesis requirement.

**Date:**

**Place:** Guide

## STATEMENT BY AUTHOR

This dissertation has been submitted in partial fulfillment of requirements for an advanced degree at Homi Bhabha National Institute (HBNI) and is deposited in the Library to be made available to borrowers under rules of the HBNI.

Brief quotations from this dissertation are allowable without special permission, provided that accurate acknowledgement of source is made. Requests for permission for extended quotation from or reproduction of this manuscript in whole or in part may be granted by the Competent Authority of HBNI when in his or her judgement the proposed use of the material is in the interests of scholarship. In all other instances, however, permission must be obtained from the author.

Subhadeep Roy

# DECLARATION

I, hereby declare that the investigation presented in the thesis has been carried out by me. The work is original and has not been submitted earlier as a whole or in part for a degree / diploma at this or any other Institution / University.

Subhadeep Roy

## List of publications arising from the thesis

### Journal

1. Soumyajyoti Biswas, Subhadeep Roy & Purusattam Ray, "*Nucleation versus percolation: Scaling criterion for failure in disordered solids*", Phys. Rev. E **91**, 050105(R) (2015).

2. Subhadeep Roy & Purusattam Ray, "*Critical behavior in fiber bundle model: A study on brittle to quasi-brittle transition*", Europhysics Letters, Volume **112**, Number 2 (2015).

### Conference Proceedings

1. S. Pradhan, A.M. Stroisz, E. Fjr, J. Stenebrten, H. K. Lund, E. F. Snsteb, S. Roy, "*Fracturing tests on reservoir rocks: Analysis of AE events and radial strain evolution*", ARMA **14-7442**.

### In Process

1. Subhadeep Roy & Sanchari Goswami, "*A Recipe for Composite Materials: An Approach through Fiber Bundle Model*", arXiv: **1510.00687**.

2. Subhadeep Roy, Soumyajyoti Biswas & Purusattam Ray, "*Failure time in heterogeneous systems*", arXiv: **1606.06062**.

3. Subhadeep Roy, Soumyajyoti Biswas & Purusattam Ray, "*Modes of failures in disordered solids*".

Subhadeep Roy

# ACKNOWLEDGEMENTS

It is my great pleasure to express my heartfelt gratitude to all those who helped and encouraged me at various stages of Ph.D.

I am indebted to my advisor Prof. Purusattam Ray for his invaluable guidance and unconditional support. Whenever any doubt/question has arisen in mind, both mathematical and non-mathematical, he has always been there to listen to me with immense patience and shown the right path. Without him, my thesis would not have seen the light of the day.

I would like to thank Soumyajyoti Biswas, Soumyadeep Bhattacharya and Sanchari Goswami for helpful discussions and encouragement.

I thank all the academic, administrative and technical members of The Institute of Mathematical Sciences, Chennai for giving a conducive environment to pursue research.

I thank my friends who made my life easier during these years with wonderful companion and lively discussions both mathematical and non mathematical. I thank my office mates for creating a wonderful office environment. I thank my friends for keeping my spirits high throughout, and for several helpful discussions.

My heartfelt thanks to my fiancee Aakriti for her emotional support and practical help.

Finally, I am forever indebted to my family specially my brother Raj for their unconditional love, care, support and encouragement.

# Contents

**1 Introduction & Motivation** **21**

1.1 Theoretical estimation of failure strength . . . . . 21

1.2 Role of defects . . . . . 23

1.2.1 Griffith's energy balance criterion . . . . . 25

1.2.2 Interaction of defects in heterogeneous materials . . . . . 26

1.2.3 Precursory activities in failure process . . . . . 29

1.3 Response of material to external stress . . . . . 32

1.4 Brittle to quasi-brittle/ductile transition . . . . . 33

1.5 Role of fracture process zone (FPZ) . . . . . 35

1.5.1 FPZ in brittle materials . . . . . 35

1.5.2 FPZ for plastic failure . . . . . 36

1.6 Aim of the thesis . . . . . 36

**2 Models of Fracture in Statistical Mechanics** **37**

2.1 Spring Network Model (SNM) . . . . . 37

2.2 Random resistor network (RRN) . . . . . 40

2.3 Fiber bundle model (FBM) . . . . . 42

**3 Effect of Disorder** **45**

3.1 Brittle to quasi-brittle transition
in fiber bundle model . . . . . 45

3.1.1 Equal load sharing scheme . . . . . 46

3.1.2 Local load sharing scheme . . . . . 54

3.2 Size effect of responses in fiber bundle model . . . . . 56

3.2.1 Equal load sharing scheme . . . . . 57

3.2.2 Local load sharing scheme . . . . . 58

3.3 Study of failure time . . . . . 62

3.3.1 Equal load sharing scheme . . . . . 62

3.3.2 Local load sharing scheme . . . . . 65

3.4 Conclusion . . . . . 65

**4 Effect of Stress Release Range** **67**

4.1 Stress release range $R$ in fiber bundle model . . . . . 68

4.2 Extreme limits of $R$ . . . . . 69

4.2.1 Cluster density . . . . . 70

4.2.2 Nucleation time . . . . . 71

4.2.3 Avalanche size distribution . . . . . 73

4.3 Scale free stress redistribution scheme . . . . . 74

4.3.1 One dimension . . . . . 75
4.3.2 Two dimension . . . . . 76
4.4 Effect of range in spring ladder model . . . . . 77
4.4.1 Simulation technique . . . . . 78
4.4.2 Abruptness in failure process . . . . . 79
4.4.3 Randomness in rupture event . . . . . 81
4.4.4 Avalanche size distribution . . . . . 82
4.5 Conclusion . . . . . 83

**5 Interplay of Stress Release Range and Disorder 84**

5.1 Description of the model . . . . . 85
5.2 Description of the phases . . . . . 85
5.3 Study of the phase boundaries . . . . . 88
5.3.1 Boundary between nucleating and percolating failure . . . . . 88
5.3.2 Boundary between abrupt and non-abrupt failure . . . . . 90
5.3.3 Boundary of high disorder regime . . . . . 91
5.4 Conclusion . . . . . 92

**6 Discussions on the thesis work 94**

**List of Figures 96**

**Bibliography 104**

# Synopsis

Fracture is a complex phenomenon involving large span of time and length scales, starting from atomic scale or laboratory scale to geological scale like earthquake. A material can break in avalanches showing precursory rupture events or catastrophically without showing such precursor. Also the rupture events might show correlation among themselves or might happen in a random manner. So the important question is: ***What are the physical criteria that govern the mode of failure ?***

Two major factors that determine the mode of fracture are disorder present in the material and the range over which the stress releases as the fracture propagates. Defects like micro cracks, dislocations or grain boundaries vastly reduce the strength of a material, as large stresses can develop at the sharp edges of these defects [1]. This is called notch effect and is the root cause of the catastrophic failure of brittle materials. Griffith suggested [2] that the typical stress, at which a sharp micro-crack of length $l$ will become unstable and grow to break the material, decreases as $1/\sqrt{l}$ [3]. This led to the weakest link of a chain concept [4, 5, 6], according to which the fracture in presence of many defects is determined primarily by the most vulnerable defect and that is how the idea of extreme statistics is applied to fracture. The other mode of fracture occurs in avalanches with constantly increasing external force. In engineering sample such avalanches [7, 8] are recorded in terms of rate of acoustic energy emission during the fracture process [9]. We have studied this effect of disorder and stress release zone in statistical mechanical models of fracture. These models for fracture of disordered solids involves the physics of threshold activated dynamical systems, self organized criticality and the physics of random field Ising model. One such model, the fiber bundle model [10, 11], consists of vertical Hokean fibers in between two parallel bars (Fig. 1). The upper bar is kept fixed

while the lower one is pulled creating a stress externally on the fibers. Each fiber is assigned a random breaking threshold, *this is the disorder in the model*. If the fiber is strained beyond the threshold, it ruptures irreversibly. The extra stress of the broken fiber is then redistributed in equal amount to either among all surviving fibers (Global load sharing scheme, GLS) or only among the nearest surviving ones (Local load sharing scheme, LLS). *These are the two extremes of stress release zone in the model*. Also there exists other redistribution methods in literature where the load is redistributed partially with global scheme and partially with local scheme. The model shows various features of critical behavior depending on the stress redistribution rule, dimensionality and strength of disorder. We aim to understand the fracture evolution in these models in the space of the above parameters and to relate the results to fracture behavior observed in nature.

## Effect of Disorder

Disorder is introduced in fiber bundle model as local fluctuation of strength of individual fibers. These strength values are chosen randomly from a distribution. We have considered mostly the uniform distribution of half width $\delta$ around the 0.5. $\delta$ is the amount of disorder in this case. We have also studied other distributions to understand the universal behavior of the model. We have considered power law distribution with exponent $-1$ within the window $10^{-\beta}$ to $10^{\beta}$, $\beta$ being the amount of disorder here. Also truncated Gaussian distribution or distribution like $x^{\beta}$ have been used. In this study of disorder the range is kept fixed at two extreme GLS and LLS limits.

In GLS scheme we have studied a critical behavior in the breakdown at a dispersion $\delta_c$ of the breaking threshold of the fibers [12]. For $\delta < \delta_c$ we find that there is a finite probability $P_b$, that rupturing of the weakest fiber leads to the failure of

the entire system. For $\delta \geq \delta_c$, $P_b = 0$. At $\delta_c, P_b \sim L^{-\eta}$, with $\eta \approx 1/3$, where $L$ is the size of the system. As $\delta \to \delta_c$, the relaxation time $\tau$ diverges obeying the finite size scaling law: $\tau \sim L^{\beta}(|\delta - \delta_c|L^{\alpha})$ with $\alpha = \beta \approx 1/3$. At $\delta_c$, the system fails, at the critical load, in avalanches (of rupturing fibers) of all sizes $s$ following the distribution $P(s) \sim s^{-\kappa}$, with $\kappa \approx 1/2$. We relate this critical behavior to brittle to quasi-brittle transition in the model. This change of behavior around $\delta_c$ is also captured in the study of fluctuation in critical stress ($\Delta\sigma_c$) and critical fraction of surviving fibers ($\Delta n_c$) [13]. $\Delta\sigma_c \sim L^{-2/3}$ and $\Delta n_c \sim L^{-1/3}$ with increasing system size $L$ for the quasi-brittle region ($\delta > \delta_c$). Below $\delta_c$ both the fluctuations decreases as $1/L$ with system size. Also above scaling of relaxation time ($\tau \sim L^{1/3}$) remains the same at critical stress in the region $\delta > \delta_c$. In brittle region ($\delta < \delta_c$) though the picture of relaxation time changes, the scaling behavior of $\tau$ remains the same but with a disorder dependent exponent: $\tau \sim L^{\gamma(\delta)}$, where $\gamma(\delta)$ decreases with $\delta$, suggesting that at low disorder the system size effect tends to vanish.

Due to the over simplification of stress redistribution in GLS scheme the extreme statistics are absent in our studies. Also the system size dependence of critical stress ($\sigma_c$) is not seen. In engineering systems sample size plays a crucial role to determine the strength of a material [14, 15, 16, 17]. The studies in GLS case is not able to produce this picture as $\sigma_c$ depends on the nature of threshold distribution only. In LLS scheme it is possible to capture these system size effects [18]. Previous work shows that $\sigma_c \sim 1/\log L$ at moderate disorder ($\delta = 0.5$) [19, 20, 21, 22, 23, 24] while at low disorder $\sigma_c$ falls rather in a scale free behavior ($\sim 1/L$) [6, 25] than logarithmic. Now from point of view of extreme statistics we know that the former behavior gives signature of Gumbel statistics while the later one of Weibull statistics. We find an intermediate disorder window where this change in scaling behavior of $\sigma_c$ takes place. Unlike GLS scheme here we did not find any particular critical disorder value ($\delta_c$) separating brittle and quasi-brittle region. Due to the system size effect in LLS scheme we can achieve abrupt failure at any disorder by simply

increasing the system size. This makes the failure of the bundle always brittle-like in thermodynamic limit ($L \to \infty$).

## Effect of Range of Stress Redistribution

To study the effect of range $R$ of stress redistribution, we have fixed the disorder at a constant value ($\delta = 0.5$, where the threshold strengths are chosen between 0 and 1) [26]. This range dependent redistribution scheme is actually an intermediate picture of GLS and LLS. According to this scheme, in 1d fiber bundle model when one fiber breaks the stress of the broken fiber is redistributed among $R$ nearest surviving neighbors on both sides. $R = 1$ will give us the localized LLS picture while on the other hand $R \sim L/2$ is the GLS or mean field limit of the model. For redistributing in two dimension we find all $R^{th}$ nearest neighbors in all directions (depending on the co-ordination number which is a function of lattice structure). Then the stress is redistributed among the fibers enclosed by all those surviving neighbors. We show that the failure mode is nucleation dominated in the large system size limit, as long as $R$ scales slower than $L^{\zeta}$, with $\zeta = 2/3$ for 1d bundle [26] and $\approx 0.82$ for 2d bundle [27]. For a faster increase in $R$, the failure properties are determined by the mean-field picture, where the damages are uncorrelated in space. In that limit, the precursory avalanches of all sizes are obtained even in the large system size limit.

## Interplay of Disorder and Range of Stress Redistribution

Now at this point a very common question can arise that: ***What happens if we tune both disorder ($\delta$) and range of stress redistribution ($R$) simultaneously ?*** More generally we can ask about the effect of disorder on above mentioned

$R_c$ value. Since already we have observed distinct behavior around $\delta_c$ we can expect the signature of a critical disorder here also.

Already we have seen that dispersion of the threshold distribution ($\delta$) is a measure of disorder. Above work is done for $\delta = 0.5$ (thresholds chosen from 0 to 1), which falls in the moderate disorder region. Here the study of critical range ($R_c$) is performed with a continuous variation of disorder within the window $0.1 < \delta < 0.5$ [**?**]. Our result shows that the above scaling ($R_c \sim L^{\zeta}$) form of $R$ with $L$ holds good for all disorder value except for the fact that for $\delta > \delta_c$ the exponent $\zeta$ remains constant at value 2/3 while below $\delta_c$, $\zeta$ becomes a function of $\delta$ and keep increasing as $\delta$ decreases. This suggest that for a constant system size ($L$), in this region ($\delta < \delta_c$) we have to go to higher and higher range value to make the rupture events uncorrelated as $\delta$ value decreases.

To achieve high disorder limit [27], instead of uniform distribution we have used power law distribution with power $-1$ from $10^{-\beta}$ to $10^{\beta}$ to assign thresholds to individual fibers. $\beta$ is the measure of disorder in this case. From the studies discussed so far two facts are quite clear that at low $\beta$ value the failure process becomes brittle like abrupt while with increasing $R$ value the fracture process becomes uncorrelated. This happens because the stress concentration favors fracture nucleation, whereas disorder favors fracture to be originated randomly over the sample. A two dimensional $R - \beta$ plane gives different regions in the model as combinations of abrupt/non-abrupt as well as correlated/uncorrelated failure.

# Study of Composite Materials

Composite materials are introduced in the field of engineering and material sciences to avoid unexpected abrupt failure in materials. In such process two or more materials with different properties are mixed in a certain proposition to get the composite

which comes with high strength and less abrupt failure than the components. In this work [28], we have studied the fracture process of a composite material in the fiber bundle model with different elastic constants, distributed randomly, as well as different random breaking strength of fibers. The critical width of the threshold distribution ($\delta_c$), for which abrupt failure occurs, is studied both analytically and numerically with increasing number of components ($k$) in the composite and it is shown that $\delta_c$ is inversely related to $k$. Corresponding phase diagram for the model suggests decrease in the tendency of abrupt fracture as number of components in the composite increase.

## Spring Bundle Model

In fiber bundle model the range of stress redistribution is put by hand and hence it does not change during the rupture processes of individual fibers. In contrast in real samples the range of interaction changes gradually in the course of fracture process. This picture is thus absent in fiber bundle model. To make the model more realistic we have studied *spring bundle model*. A spring bundle model consists of Hookean springs organized in the form of a ladder. The Hamiltonian for the model can be written as:

$$H = \frac{1}{2}\left[k_r \sum_{\langle ij \rangle} \delta r^2 + k_\alpha \sum_{\langle ij \rangle} \delta\alpha^2\right]$$

where $k_r$ and $k_\alpha$ are respectively linear and angular force constant. Also $\delta r = (r - r_0)$, $\delta\alpha = (\alpha - \alpha_0)$, $r_0$ and $\alpha_0$ being the length of spring and intermediate angle between two adjacent springs at equilibrium position. The sum goes over all nearest neighbor $\langle ij \rangle$ pairs. This model with disorder $\delta$ of the breaking thresholds of the springs is studied for various angular force constant $k_\alpha$ [29]. For small $k_\alpha$ we find the fracture is of nucleating type and for high $k_\alpha$ the fracture of springs becomes uncorrelated. We find three distinct regions: nucleating, percolating and crossover region. Abruptness

of fracture, critical stress, avalanche size distribution and fluctuation in stress profile of the springs are studied to characterize the regions. Similar model has been studied before also [30, 31].

## Study of Acoustic Emission Experiment

Fracturing in reservoir rocks is an important issue for the petroleum industry - as productivity can be enhanced by a controlled fracturing operation. Fracturing also has a big impact on $CO^2$ storage, geothermal installation and gas production at and from the reservoir rocks. Therefore, understanding the fracturing behavior of different types of reservoir rocks is a basic need for planning field operations towards these activities. In our study [9], the fracturing of rock sample is monitored by Acoustic Emission (AE) and post-experiment Computer Tomography (CT) scans. The fracturing experiments have been performed on hollow cylinder cores of different rocks - sandstones and chalks. Our analysis show that the amplitudes and energies of acoustic events clearly indicate initiation and propagation of the main fractures. The amplitudes of AE events follow an exponential distribution while the energies follow a power law distribution. Time-evolution of the radial strain measured in the fracturing-test will later be compared to model predictions of fracture size.

# Bibliography


[1] G. E. Dieter, *Mechanical Metallurgy* (Metric Editions, Materials Science & Metallurgy) (1993).

[2] B. Lawn, *Fracture of Brittle Solids* (Cambridge Solid State Science Series, Second edition) (1995).

[3] Zdenek P. Bazant, Probabilistic Engineering Mechanics **19**, 307-319 (2004).

[4] M.Tanaka, R.Kato, and A.Kayama, Journal of materials science **37**, 3945-3951 (2002).

[5] F. A. McClintock, *Statistics of Brittle Fracture, in The Fracture Mechanics of Ceramics*, edited by Bradt R. C. et al., Vol. I (Springer-Verlag, US), p. **93** (1974).

[6] P. Ray and B. K. Chakrabarti, Solid State Commun., **53**, 477 (1985).

[7] A. Petri, G. Paparo, A. Vespignani, A. Alippi, and M. Costantini, Phys. Rev. Lett. **73**, 3423 (1994).

[8] A. Garcimartn, A. Guarino, L. Bellon, and S. Ciliberto, Phys. Rev. Lett **79**, 3202 (1997).

[9] S. Pradhan, A.M. Stroisz, E. Fjr, J. Stenebrten, H. K. Lund, E. F. Snsteb, S. Roy, ARMA **14-7442** (2014), arXiv:**1512.05184** (2015).

[10] S. Pradhan, A. Hansen and B. K. Chakrabarti, Rev. Mod. Phys. **82**, 499 (2010).

[11] F. T. Pierce, J. Text. Ind. **17**, 355 (1926).

[12] S. Roy and P. Ray, Europhysics Letters, **112**, 26004 (2015).

[13] S. Roy, S. Biswas and P.Ray, arXiv:**1606.06062** (2016).

[14] Z. P. Bazant, S. D. Pang, M. Vorechovsky, D. Novak, R. Pulk, Fracture Mechanics of Concrete Structures, Li et al (eds) Ia-FraMCos, ISBN **0 87031 135 2**, (2004).

[15] S. G. Bardenhagen, J. U. Brackbill and D. Sulsky, Phys. Rev.E **62**, 3 (2000).

[16] A. Carpinteri, Int. J. Solids Structures 31, No. **3**, 291-302 (1994).

[17] W. A. Curtin, Phys. Rev. Lett. **80**, 1445 (1998).

[18] S. Roy, "*Size effects in local load sharing fiber bundle model with continuous variation of disorder*", in preparation.

[19] M. Kloster, A. Hansen, and P. C. Hemmer, Phys. Rev. E **56**, 2615 (1997).

[20] S. D. Zhang and E. J. Ding, J. Phys. A **28**, 4323 (1995).

[21] S. D. Zhang, E. J. Ding, Phys. Rev. B **53**, 646 (1996).

[22] D. G. Harlow and S. L. Phoenix, J. Mech. Phys. Solids **39**, 173 (1991).

[23] P. M. Duxbury, and P. M. Leath, Phys. Rev. B **49**, 12676 (1994).

[24] P. M. Duxbury and P. L. Leath, J. Phys. **A20**, L411 (1987).

[25] S. Pradhan, and A. Hansen, Phys. Rev. E **72**, 026111 (2005).

[26] S. Biswas, S. Roy and P. Ray, Phys. Rev. E, **91**, 050105(R) (2015).

[27] S. Roy, S. Biswas, P. Ray, "*Modes of failures in disordered solids*", in preparation.

[28] S. Roy and S. Goswami, arXiv: **1510.00687** (2015).

[29] S. Venkatesan, S. Roy and P. Ray, "*Nucleation versus percolation scenario in fracture: a molecular dynamics simulation study in spring bundle model*", in preparation.

[30] W. A. Curtin and H. Scher, Phys. Rev. Lett. **67**, 2457 (1993).

[31] Knut S. Gjerden, Arne Stormo and Alex Hansen, Phys. Rev. Lett. **111**, 135502 (2013).

# Chapter 1

# Introduction & Motivation

Fracture in heterogeneous materials takes place through initiation, growth, coalescence and propagation of the micro-cracks, which leads to the final failure of materials. Failure of materials have received lots of attention in the field of physics, engineering and material science over the last decade [1, 2, 3].

## 1.1 Theoretical estimation of failure strength

One of the main aim of fracture studies is to estimate the strength and predict the failure of materials. In the literature there are many studies to find the strength of materials. In the early days, the cohesive force between the atoms was considered to be the origin of strength of materials [4]. As an approximation, one can assume the cohesive force between the atoms to follow a sine curve (as an outcome of the interplay between repulsive and attractive force between atoms). Let us assume that, $\lambda$ is the wavelength of cohesive force curve and $\sigma_{max}$ is the maximum of the cohesive force curve, which is basically the theoretical cohesive strength. This behavior is

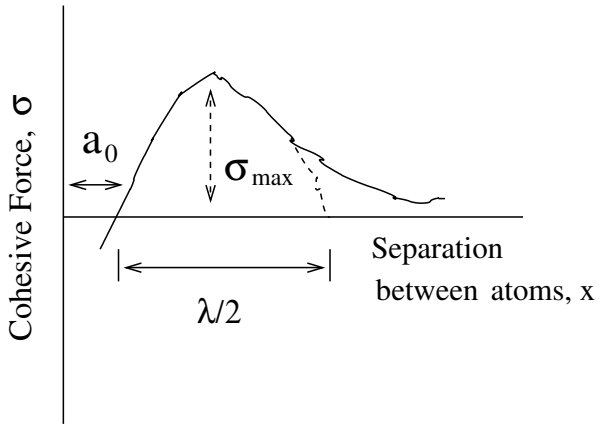


Figure 1.1: Variation of cohesive stress with increasing separation between atoms. $a_0$ is the inter atomic spacing at unstrained condition.

shown in figure 1.1. Then the cohesive strength will be given by

$$\sigma = \sigma_{max} \sin\left(\frac{2\pi x}{\lambda}\right) \tag{1.1}$$

Now, work done during the fracture process will be the area under the cohesive curve given by :

$$\begin{aligned} W =& \int_0^{\lambda/2} \sigma_{max} \sin\left(\frac{2\pi x}{\lambda}\right) dx \\ =& \frac{\lambda \sigma_{max}}{\pi} \end{aligned} \tag{1.2}$$

This work done finally goes into creating to new fracture surface and helps the crack to propagate. Surface energy required for this new fracture surface will be $2\Gamma$, where $\Gamma$ is the energy per unit area for the new surface. The factor 2 comes from the two surfaces, that are produced from the growth of the crack. Equating the work done with surface energy, we get

$$\begin{aligned} \frac{\lambda \sigma_{max}}{\pi} &= 2\Gamma \\ \sigma_{max} &= \frac{2\pi\Gamma}{\lambda} \end{aligned} \tag{1.3}$$

where $E$ is the elastic constant of the material and $a_0$ is the inter-atomic spacing at unstained condition (see figure 1.1). Hooke's law is valid for small displacement $x$ where we can then write: $\sigma = \frac{Ex}{a_0}$. Taking derivative of this $\sigma$ w.r.t $x$ and equating it with the derivative obtained from Eq.1.1 we get, in small $x$ limit

$$\sigma_{max}\frac{2\pi}{\lambda} = \frac{E}{a_0} \tag{1.4}$$

Comparing Eq.1.3 and Eq.1.4, we obtain an expression for theoretical cohesive strength to be

$$\sigma_{max} = \left(\frac{E\Gamma}{a_0}\right)^{1/2} \tag{1.5}$$

This expression for cohesive strength of materials seems quite convincing until it meets the experimental outcome. Experimentally the strength of materials are observed to be much low (of the order of 1000) than their theoretical values. This discrepancy happens because of existence of defects within materials.

## 1.2 Role of defects

Defects like micro-cracks and dislocations play crucial role in fracture process of materials. As discussed above the existence of such defects decreases the strength of any material by huge amount. Below we have discussed the effect of dislocation and micro-cracks.

**Effect of dislocation :**

Fracture in ductile material is caused by slip through crystal planes. A moving defect like dislocation enhances the tendency of such slip in planes [5, 6]. Motion of dislocation through crystal planes is guided by many parameters like width of

dislocation, existence of grain boundaries, temperature, applied stress etc. Figure

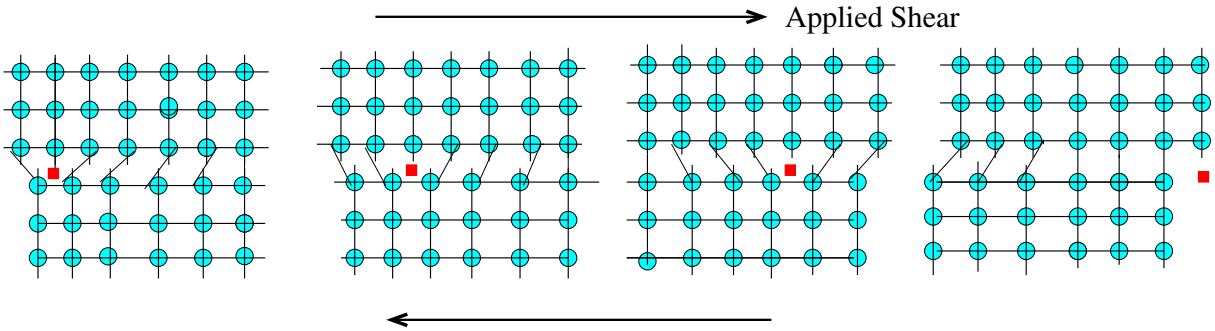


Figure 1.2: Motion of a dislocation through crystal plane is shown in the figure. This motion leads to slip in between the planes.

1.2 shows the motion of a dislocation through crystal plane creating a slip. The red cube gives the position of the dislocation. As the dislocation moves to the right direction it help the upper plane to slide over the lower one. Due to such motion the slip between planes occurs much lower stress than the theoretical predicted value.

**Effect of micro-crack :**

Existence of micro-crack enhances the local stress profile at the notch of the crack and local stress near the tip of the micro-cracks are much higher than the applied stress. The scenario is shown in the figure 1.3. Green line shows the local stress value $\sigma_n$, near the notch while a constant stress $\sigma_{ext}$ is applied externally. The

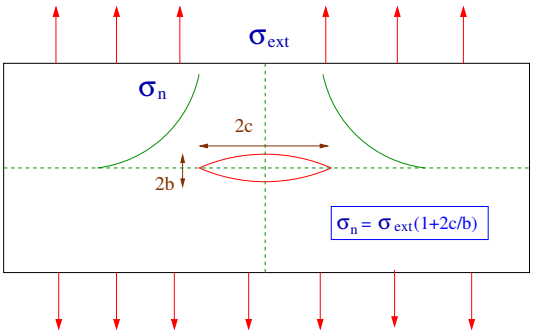


Figure 1.3: Notch effect in real system is shown in the figure. The stress at the edges of the crack is much higher than the external stress,0 depending on the major (c) and minor axes (b) of the elliptical crack.

shape of a crack is approximated to be elliptic with minor axes b and major axes c

respectively. The stress on the notch of a elliptic crack of length 2c and radius of curvature $\rho$ is given by Orowan and Inglis [7, 8]

$$\sigma_n = 2\sigma_{ext}\left(\frac{c}{\rho}\right)^{1/2} \tag{1.6}$$

The stress at the tip will be higher for a larger crack with smaller radius of curvature. The criterion for a crack to propagate is given by Griffith through energy balance condition. This is discussed in the next section.

### 1.2.1 Griffith's energy balance criterion

For a typical crack model (shown in fig.1.3), where the crack is approximated by an ellipse of major axes 2c (also it is the crack length), we get the elastic strain energy (plate of unit thickness) to be :

$$U_{elastic} = -\frac{\pi\sigma^2 c^2}{E} \tag{1.7}$$

where $E$ is the elastic modulus of the material and $\sigma$ is the tensile stress. The negative sign stands for the release of the energy. On the other hand the surface energy due to the crack is

$$U_{surface} = 4c\Gamma \tag{1.8}$$

So the total change in energy as a result of the creation of the crack is

$$U_{total} = U_{elastic} + U_{surface} \tag{1.9}$$

Now Griffith's energy balance criteria [9] states: *A crack will propagate if elastic strain energy is compensated by the surface energy.*

Then satisfying above condition, for further increment $dc$ of a crack of length $c$, we get

$$\frac{dU_{total}}{dc} = 0$$
$$\sigma = \left(\frac{2E\gamma}{\pi c}\right)^{1/2} \tag{1.10}$$

Above expression for strength of materials shows a quite good agreement with experimental results and can predict the variation of strength with crack length, satisfactorily for brittle materials such as ceramics or glass [10, 11], metal whiskers [12] etc.

Though Griffith's energy balance treatment can offer an insight to the crack propagation, there are some issues that can not be resolved by this critaria:

- Volume or system size dependence of the strength
- Roughness of fracture surface
- Avalanche behavior before final rupture

This discrepancy happens because real materials do not consist of a single defect or micro-crack, as it was assumed in Griffith's criterion. Instead, the failure happens in real systems as cumulative effect of all defects present in

### 1.2.2 Interaction of defects in heterogeneous materials

The issues mentioned above can not be answered through Griffith's criteria since failure process in materials is quite different from the theoretical approach. In fracture process the material properties like strength, failure time etc. are non-self-averaging, as the failure is determined by the weakest defect or the most vulnerable crack [13, 14, 15]. Due to this, a large scatter in material properties, mainly in

fracture strength, is seen. Also the strength decreases with the system size. The system size effect of materials on strength of failure is discussed in [16].

Many studies have been performed on the system size effect on strength of real materials like: sea ice [17], concrete [18, 19], carbon composite [20] etc. In these cases the strength of the material was observed to decrease with system size in a scale free behavior with exponent close to $-1/2$. This scale free behavior is a direct evidence of Weibull distribution of strength values. Though quite rarely but another distribution for strength of materials are found, namely the Gumbell distribution. Experimental results [21], performed on a cylindrical silica extrudates with pore volume up to 80% and median pore diameter around $100nm$, shows that the distribution for the strength matches with Gumbell distribution much better than Weibull distribution. Below an analytical approach for heterogeneous materials is given, explaining the conditions under which we get Weibull and Gumbel distribution for threshold strength.

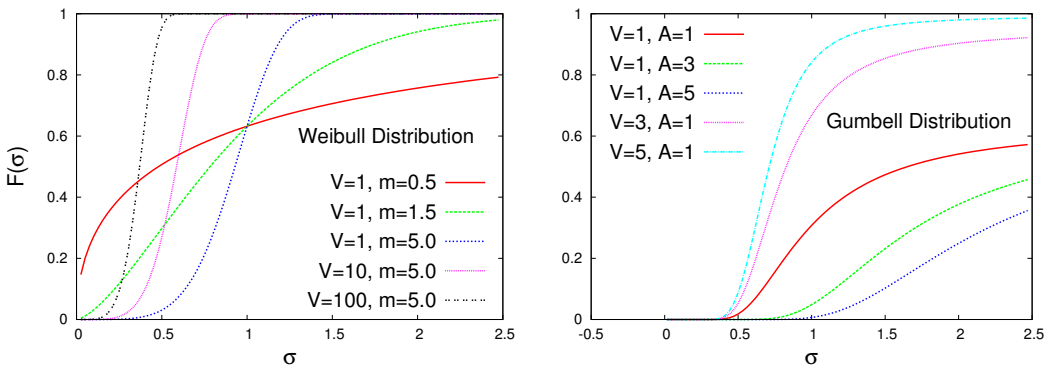


Figure 1.4: Above figures shows the failure probability, $F(\sigma)$, of materials at low disorder limit (Eq.1.12, left figure) and intermediate disorder limit (Eq.1.13, right figure). In both limits, $F(\sigma)$ increase as we go to higher stress values. The rate of this increase is faster for higher volume $V$.

Materials (mostly heterogeneous) under experiments do not contain a single micro-crack or defect. Instead in heterogeneous materials there are several number of micro cracks and defects which play their individual role to the failure process. As a result, the defects cannot be treated individually and the failure happens as a

cumulative effect of those defects [22]. If we consider a sample of volume $V$ under a stress $\sigma$ with $n$ independent faults then:

$$\begin{aligned} 1 - F(\sigma) &= \prod_{1}^{n} (1 - f(\sigma_i)) \\ &\cong \exp\left[ - \sum_{i} f(\sigma_i) \right] \\ &\cong \exp\left[ -V p(\sigma) \right] \end{aligned} \tag{1.11}$$

where $f(\sigma_i)$ and $F(\sigma)$ are failure probability of individual defects of the material under stress $\sigma$ respectively. Here, $p(\sigma)$ is the density of flaws weaker than $\sigma$. Below we have discussed two different cases, explaining how we get this two distributions for threshold strength.

**Low defect concentration**

If we assume that defects of all scales are involve in the fracture process of the material, then the flaw density $p(\sigma)$ will be given by: $c\sigma^m$. $c$ and $m$ are constants. In that case from Eq.1.11 we get

$$F(\sigma) = 1 - \exp(-V\sigma^m) \tag{1.12}$$

This is a Weibull distribution with Weibull constant $m$. The average strength of the material goes with the volume as : $\langle \sigma \rangle \sim V^{-m}$ [13]. If $L$ is the system size and $d$ is the dimension of the material then, $\langle \sigma \rangle \sim L^{-dm}$. This matches with the scale free behavior of failure strength, explored by Bazant, with increasing system sizes [23].

**Intermediate defect concentration**

If we assume that the defects of a particular characteristic dimension $c$ (in other word the crack length) only responsible for development of fracture, we get $p(\sigma) \sim \exp(-cA)$ where $A$ is constant. Now from Griffith's law (Eq.1.10) we can write: $c \sim 1/\sigma^2$. This gives us the Gaussian distribution for threshold stress

$$F(\sigma) = 1 - \exp\left[-V \exp\left(-\frac{A}{\sigma^2}\right)\right] \tag{1.13}$$

In this case the average strength falls in a inverse logarithmic behavior with the volume ($\langle\sigma\rangle \sim c/\sqrt{logV}$) [24].

For both the distributions the failure probability increases with increasing $\sigma$ value (Figure 1.4). The rate of increase is faster as we go to higher volume $V$. Most probably, this happens because in a bigger sample the probability of having a larger and weaker defect is higher. As a result the most probable value of failure stress decreases when volume is increased [25, 26].

### 1.2.3 Precursory activities in failure process

Fracture processes, which are guided by accumulation of defects, shows precursor activities and avalanches with applied stress [27]. As the strength of a heterogeneous material varies from point to point, on application of external stress the weakest part breaks first. This increases stress on other parts of the material and that part can further break, starting an avalanche. Such avalanche might break the total material or might require increment of external stress where the material goes through a number of avalanches. These avalanches and precursor activities are studied through acoustic emission experiment [28, 29, 30]. The schematic diagram for the experimental set up and acoustic emission data is shown in figure 1.5. A

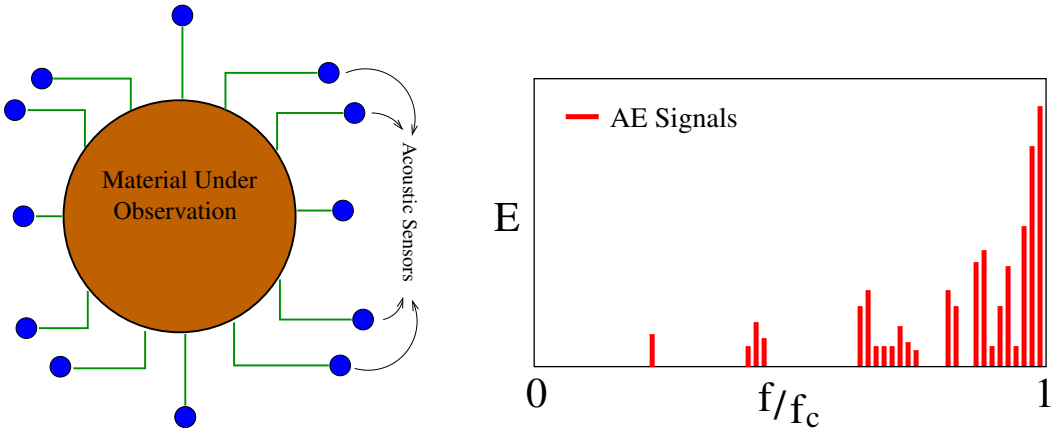


Figure 1.5: Left: Experimental set up for acoustic emission experiment. A number of acoustic sensors are attached to the material. The energy release in fracture process is recorded through these sensors.
Right: AE signals collected through the sensors. Energy emitted in failure process is plotted against the applied stress value. The density of signal is very high near the failure point.

number of acoustic sensors are connected with the material. A fraction of elastic energy, released during fracture process in form of sound, is captured through these sensors. These energy values as shown in figure 1.5 with increasing stress ($f$) values. The population of signals is quite high close to the failure point ($f \to f_c$). The main observations of the experiment are: (i) size distribution of energy emitted and (ii) distribution of burst interval. From these studies of avalanches with increasing external stress, we get the following results

1. $E \sim (f - f_c)^{-\gamma}$, where $E$ is the energy emitted in fracture process. $f$ is the applied stress and $f_c$ is the critical stress, at which the material breaks.

2. $P(E) \sim E^{-\alpha}$. $P(E)$ is the probability distribution for the energy emitted.

3. $C(\delta t) \sim (\delta t)^{-\beta}$. $\delta t$ is interval between two consecutive burst. $C(\delta t)$ is distribution for $\delta t$.

Above scaling laws were found to have universal behavior with universal exponents $\gamma$, $\alpha$ and $\beta$. Experimental results are given in a tabular form below showing the

exponent values.

| Materials | $\gamma$ | $\alpha$ | $\beta$ |
|---|---|---|---|
| Chipboard wood (Ref. [31]) | $0.27 \pm 0.05$ | $1.9 \pm 0.1$ | $1.15 \pm 0.05$ |
| Synthetic plaster (Ref. [28]) | – | $1.3 \pm 0.1$ | $0.4 \pm 0.1$ |
| Composite materials (Ref. [32]) | $0.28 \pm 0.05$ | $1.9 \pm 0.1$ | $1.55 \pm 0.05$ |
| Cellular glass (Ref. [33]) | – | $1.5 \pm 0.1$ | $1.27 \pm 0.01$ |

In a recent study we have observed the energy release in fracture as a function of time, instead of applied stress [34]. Same scale free behavior was found for the distribution of energy. Experiments are performed with many stones like lixhe chalk, barea, castlegate, red wildmoor etc. and value of the universal exponent $\alpha$ was found between 1.0 and 2.0 [34].

Materials like glass, ceramics etc. break in a single avalanche, almost equal to its volume, prior to global failure. No increment of external stress is required to break such materials. These materials are known as brittle materials. For other two categories of materials, quasi-brittle and ductile, many small avalanches take place with increasing external stress. These different nature of avalanche behavior for brittle and quasi-brittle/ductile materials is also get reflected through there response to external stress. We have discussed these responses in details in the next section.

## 1.3 Response of material to external stress

As we have already seen in the above section, depending on failure process we mainly get three types of materials: brittle, quasi-brittle and ductile. These materials along with their response to external stress is discussed below.

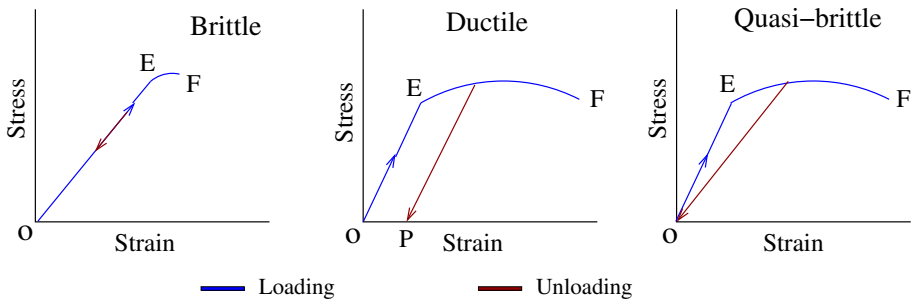


Figure 1.6: Response curve of brittle, quasi-brittle and ductile materials. Brittle materials show perfectly linear response prior to an abrupt failure. Both quasi-brittle and ductile materials have appreciable plastic region. Only difference is ductile materials show permanent deformation even when the applied stress is withdrawn.

- **Brittle materials :** In brittle materials the fracture is guided by the progress of the weakest or vulnerable defect (micro-crack) in the material. Crack in brittle materials propagates very fast and we get no warning prior to global failure. The response curve for these materials only includes elastic region (OE in figure 1.6) and negligible amount of elongation or strain (EF in figure 1.6) is observed during the fracture process.

- **Quasi-brittle/ductile materials :** In quasi-brittle or ductile materials the failure happens as a collective effect of many defects and thus the response curve shows both linear or elastic region and plastic region. These materials show sufficient elongation (EF in figure 1.6) prior to global failure. The only deference is quasi-brittle material does not sustain any permanent deformation (OP in figure 1.6) after unloading of external stress like ductile material does.

In ductile materials we get very high strain and cup cone like necking behavior before the failure. In comparison for brittle materials the fracture surface is flat and do not show any stretching [1, 4, 35].

## 1.4 Brittle to quasi-brittle/ductile transition

We have already seen in the above two sections that brittle and quasi-brittle/ductile materials have very different properties. Brittle materials break abruptly in a single avalanche. Strength of the material is high but toughness (strain) is very low. A very small amount of energy (amount energy released is basically the area under the stress v/s strain curve) is released during the failure process of such materials. On the other hand in case of quasi-brittle or ductile materials, the material breaks in a number of successive avalanches with increasing applied stress. Since the failure process is guided by cumulative effect of all defects, a huge amount of energy is released in the fracture process.

Though strength and failure process of brittle, quasi-brittle or ductile materials are very different from each other, they are not inherent properties of the materials and changes a lot with external parameters like temperature, pressure, porosity, strain rate etc. This change in behavior with certain external parameter is known as brittle to quasi-brittle/ductile transition.

- **Effect of temperature :** Low temperature embrittlement is commonly seen in many materials. It is observed experimentally [36, 37] that ductile materials can show proper linear response and abrupt failure like brittle materials if it is brought below a critical temperature ($T_c$). Around this $T_c$ the energy releases due to failure process (area under the response curve) shows sudden fall (Fig.1.7) as the motion of defects like dislocation is ceased and the materials stop showing plastic response.

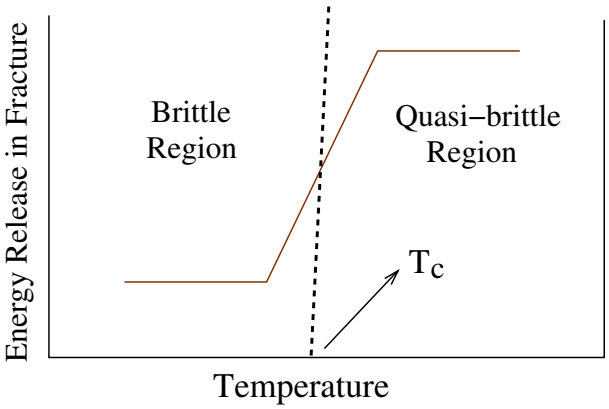


Figure 1.7: The figure shows brittle to ductile transition with varying temperature. The energy release in fracture process falls very rapidly around a critical temperature $T_c$ which is the brittle to ductile transition point.

- **Effect of pressure :** Another parameter guiding this transition apart from temperature is the pressure applied on the material. In rocks, a transition is seen at high confining pressure from brittle to ductile material. [36, 37].

- **Role of dislocation :** We already know that the origin of plastic response in material is motion of dislocations. A dislocation motion dependent brittle to quasi-brittle/ductile transition is observed experimentally in doped silicon [38] and tungsten single crystals [39].

- **Effect of porosity :** Such a transition from brittle to quasi-brittle material in random porous Au was observed in Ref. [40]. The transition is observed with varying micro structural length scale.

There are many attempts in the literature to design statistical mechanical models for describing brittle to ductile transition (BDT). In some models BDT is observed as an effect of nucleation of single dislocation [41, 42, 43] or by the motion of a group of dislocations [38, 44, 45]. Later Khantha et al. has studied this effect of dislocation [46] along with the effect of strain rate on BDT temperature [47]. Recently by Picallo et al., a brittle to ductile transition was observed in random fuse network, where it was assumed that a resistance can go through a number of healing cycles before it

breaks and starts behaving like insulator. BDT was observed as a function of these healing cycles [48]. Langer and Lobkovsky has studied BDT in a one-dimensional model that obeys viscoplastic constitutive equations [49]. Experiment as well as simulation in continuum mechanical model was performed recently, where a brittle to quasi-brittle transition was observed with varying crack initiation velocity [50].

## 1.5 Role of fracture process zone (FPZ)

Not only disorder but also the stress release range [51] is another factor that guides the nature of failure. This stress release range is mainly determined from the fracture process zone (FPZ) near the crack tip. In this FPZ the energy due to the fracture process stored and used to create new fracture surface and helps the crack to propagate [52, 53, 54]. Depending on the sharpness of the crack tip (Fig.1.8), which is a measure of the area of FPZ, a material breaks by either nucleation or through a series of precursory events. This fracture process zone is basically the range up to which the information of a particular defect can travel.

### 1.5.1 FPZ in brittle materials

Figure 1.8 shows the crack tip and FPZ in case of brittle fracture and plastic fracture (quasi-brittle or ductile). Brittle materials does not show any such FPZ and the total energy due to failure is concentrated on the crack tip only. As a result, the FPZ can not effect any other micro-cracks and propagation of crack takes place from the initial one only.

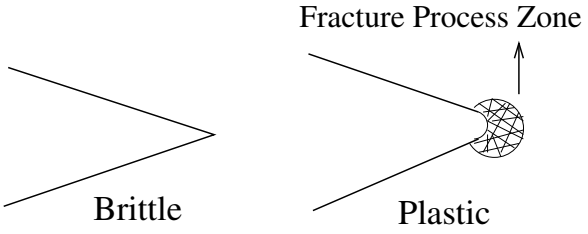


Figure 1.8: Fracture process zone (FPZ) near the crack tip for brittle and plastic failure is shown. Brittle cracks hardly shows any FPZ while one the other hand in case of plastic failure we get certain amount of FPZ within which the energy due to fracture process is stored.

### 1.5.2 FPZ for plastic failure

More blunt the crack tip is, it leads to increasing area of FPZ. In that case the increasing FPZ might include other cracks and the fracture might start propagating from the second crack rather than the previous one. Materials like ductile, with blunt crack tip and appreciable amount of FPZ, break continuously with cumulative effect of many defects and thus show plastic region and deformation in the response curve.

## 1.6 Aim of the thesis

The thesis comprises the study of the effect of the disorder and stress release range on the development and morphology of fracture. We have worked on mainly fibers bundle model, which is a very simple and useful model to study failure process. This model is studied with varying disorder and stress release range to observe fracture abruptness, strength, fracture pattern, size effects and many other aspects and compare the results with real systems. In addition, we have studied another model of fracture process, namely spring ladder model, by controlling the stress release range through the angular elastic constant.

# Chapter 2

# Models of Fracture in Statistical Mechanics

There are many models which has been adopted in the literature to design and describe fracture phenomena. Stochastic behavior in these models are introduced as fluctuation of local parameters. These models are proven to give sufficient information about strength, fracture abruptness, rupture pattern and many other aspects. Examples of such three fracture models in statistical mechanics are given below in a decreasing order of computational complexity:

1. Spring network model
2. Random resistor network
3. Fiber bundle model

## 2.1 Spring Network Model (SNM)

Spring network model [55, 56] is the tensorial approach to understand failure process. In this model not only the magnitude but also the direction of applied stress matters

a lot to determine the failure. This model consist of a network, where all bonds are Hookean springs with linear force constant $k_s$. Apart from this, there are two other parameters that characterize the behavior of the springs: length of the spring at unstrained condition ($r_0$) and the critical strain of a spring ($r_c - r_0$), above which it breaks irreversibly. $r_c$ is the length of the spring just before rupture. There is also another parameter that takes care of the shear stress on the bundle, the angular force constant $k_\alpha$. At unstrained condition, the angle between two springs adjacent

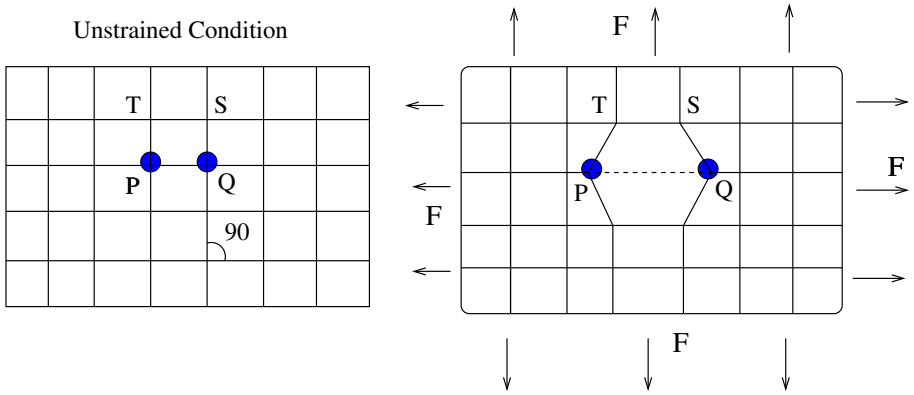


Figure 2.1: A two dimensional spring network model is shown, at both unstrained condition (left) and with a spring broken due to the application of external force (right).

to a particular node is, $\alpha_0 = 90^\circ$ (see figure 2.1), if the network a is square or cubic lattice. Altogether the Hamiltonian of the system will be given by:

$$H = \frac{1}{2} \sum_{\langle ij \rangle} k_s (r - r_0)^2 + k_\alpha (\alpha - \alpha_0)^2 \tag{2.1}$$

The sum goes over all nearest neighboring pairs $\langle ij \rangle$. $r$ and $\alpha$ are respectively the length of a spring and angle between two springs at a node, for particular strained condition. Initially, the model does not cause any energy cost since $r = r_0$ and $\alpha = \alpha_0$. Due to the application of external force, if any spring ($PQ$ in figure 2.1) breaks, it leads to a change in the parameters of Hamiltonian : $k_s = 0$ and $k_\alpha$ involving the broken spring becomes 0. The force applied on each node then get changed due to this single rupture. This modified in applied force leads to different

positioning of every node and hence the length of the springs get changed. One of the very simple hence very useful algorithm to assign new positions to the nodes is '*Verlet algorithm*'. This algorithm is discussed below in details.

**Verlet algorithm**

Let's assume, at time $t_0$, the position of a node is $\vec{x}_0$, velocity is $\vec{v}_0$ and acceleration is $\vec{a}_0$. Then, at next time step, $t + \Delta t$, the position of that node will be

$$\vec{x}_1 = \vec{x}_0 + \vec{v}_0 \Delta t + \frac{1}{2}\vec{a}_0 (\Delta t)^2 \tag{2.2}$$

Generalizing above equation for any particular time $t$, we get

$$\vec{x}(t + \Delta t) = \vec{x}(t) + \vec{v}(t)\Delta t + \frac{1}{2}\vec{a}(t)(\Delta t)^2 + O(\Delta t^3) + O(\Delta t^4) \tag{2.3}$$

Replacing $\Delta t$ by $-\Delta t$, we get

$$\vec{x}(t - \Delta t) = \vec{x}(t) - \vec{v}(t)\Delta t + \frac{1}{2}\vec{a}(t)(\Delta t)^2 - O(\Delta t^3) + O(\Delta t^4) \tag{2.4}$$

Adding Eq.2.3 and Eq.2.3 we get,

$$\vec{x}(t + \Delta t) = 2\vec{x}(t) - \vec{x}(t - \Delta t) + \vec{a}(t)(\Delta t)^2 + O(\Delta t^4) \tag{2.5}$$

Neglecting higher order term in $\Delta t$ and using $\vec{a}(t) = \vec{f}(t)/m$, we can write

$$\vec{x}(t + \Delta t) = 2\vec{x}(t) - \vec{x}(t - \Delta t) + \frac{\vec{f}(t)}{m}(\Delta t)^2 \tag{2.6}$$

where $\vec{f}(t)$ is the force applied on that node at time $t$. By above algorithm after the breaking of a certain node, all other nodes move to a new positions, depending on how much force is applied on it.

Due to this new positioning of the nodes, there might be further breaking of springs, and the redistribution goes on, until either the model breaks or reaches to a stable state. In the later case, the external force is increased to make the model evolve further. This force increment goes on until the complete model fails.

The model is quite realistic as it is the closest discrete version of continuum elastic manifold. However, the simulation is difficult as $\Delta t$, in principle, should be extremely small. Otherwise, one encounters with unrealistic oscillations and the system does not reach equilibrium. On other hand, small $\Delta t$ increases the relaxation time. Various techniques, like applying artificial damping, is used for the fast equilibration of the system without experiencing any unwanted oscillations.

## 2.2 Random resistor network (RRN)

This is an electrical analog of designing fracture process [57, 58, 59]. It consists of a 2d tilted square lattice where all the bonds are resistors with unit resistances. A constant potential difference is applied through one direction of the bundle. On the other direction, perpendicular to it, a periodic boundary condition is applied. All

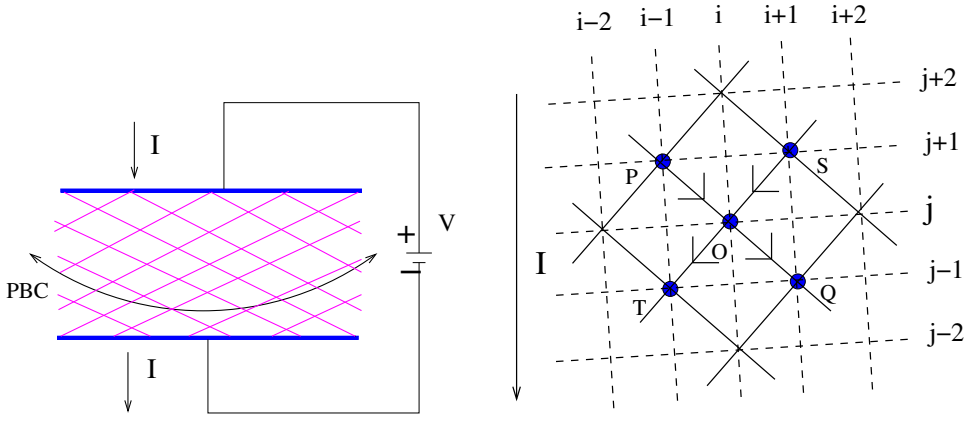


Figure 2.2: Left: 2d inverted square lattice shaped random resistor network. A potential deference $V$ is applied to the model creating a current flow $I$.
Right: A particular mess of involving five lattice point is observed to explain the breaking criterion and redistribution.

this resistors have certain threshold chosen randomly. Resistances of all resistors are same. Figure 2.2 shows a schematic diagram of random resistor network (left), explaining the Kirchhoff's law of current flow, through every node (right).

If we consider a mesh with 5 nodes $P$, $Q$, $T$, $S$ and $O$ with potential $V_P$, $V_Q$, $V_T$, $V_S$ and $V_O$ respectively, then according to Kirchhoff's law, current through the resistor joining node $P$ and $O$ will be $I_{PO} = (V_P - V_O)R_{PO}$. $I_{PO}$ is the current flowing from node $P$ to node $O$ and $R_{PO}$ is the resistance of the resistor joining node $P$ and $O$. Similarly $I_{OT} = (V_T - V_O)R_{OT}$. Since the current is flowing outward from node $O$, the sign of $I_{OT}$ will be negative.

If current through any resistor crosses any random threshold limit, that resistor burns irreversibly and starts acting as a insulator (resistance is infinite). After this rupture we solve Kirchhoff's law to assign new potentials to each node. This new potentials are assigned by Kirchhoff's law, that states, sum of the current flow through each node will be zero. By this, we get

$$\begin{aligned} & I_{PO} + I_{SO} + I_{OT} + I_{OQ} = 0 \\ & or, \frac{(V_P - V_O)}{R_{PO}} + \frac{(V_S - V_O)}{R_{SO}} + \frac{(V_T - V_O)}{R_{OT}} + \frac{(V_Q - V_O)}{R_{OQ}} = 0 \end{aligned} \tag{2.7}$$

If any resistor breaks, it is treated as an insulator and the resistance is taken to be infinity. When a resistor breaks, the current law, given by Eq. 2.7, gets modified new potential is assigned to each node. Due to redistribution through Kirchhoff's law there might be further breaking triggering an avalanche of ruptures. After each and every rupture, we go on solving Kirchhoff's law until the model comes to equilibrium, when the potentials on the nodes become constant. After the equilibrium is reached, the applied potential difference is increased to create further breaking and redistribution. This process goes on unless a series of broken resistors percolates through the model giving zero current.

Random resistor network is very useful model in statistical mechanics to study fracture and breakdown phenomena. There are many studies carried out on RRN model regarding strength of the model, abruptness in failure process, study of fracture path etc. As already discussed in chapter 1, a brittle to ductile transition was observed recently in RRN model [48]. Apart from that, damage in the model through nucleating crack growth and percolating crack growth was also observed [57, 58, 59]. However, it was recently noted that apart from extremely high disorder [60] the damage nucleation is always the final mode of fracture.

Random resistor network model, unlike the tensorial spring network model, is scalar model. The main problem one encounters here is equilibrium time. As more and more resistors become insulator, the equilibrium time increases. One uses Conjugate gradient method [61, 62], Fast Fourier transformation [57, 63] to achieve fast equilibration.

## 2.3 Fiber bundle model (FBM)

Fiber bundle model [64, 65] is perhaps the simplest model to study fracture. The model consists essentially of fibers attached between two parallel bars. We consider here only Hookean fibers, though, in general, any stress-strain constitutive relation can be obeyed by them. The bars are pulled apart with a force which induces a stress on the fibers. Each fiber sustains a stress up to a threshold (chosen randomly from a distribution) beyond which it breaks irreversibly. Once a fiber breaks, the stress of the fiber is redistributed among other surviving fibers. For such redistribution mainly two schemes has been adopted in the literature: equal load sharing scheme (ELS) [66, 67] and local load sharing scheme (LLS) [68, 69, 70, 71, 72, 73].

- ELS scheme : If the stress of a broken fiber is distributed equally among all the surviving fibers, the model is called the equal load sharing (ELS) model.

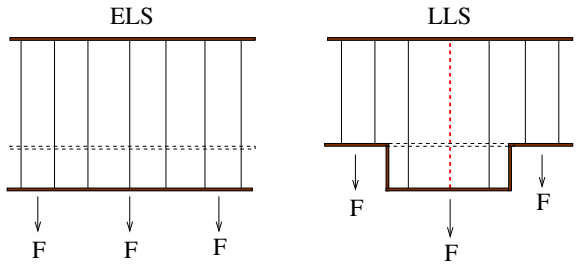


Figure 2.3: Fiber Bundle Model : Hookean fibers with random thresholds attached between two parallel bars. The figure shows the behavior of the bars in case of equal load sharing (ELS) and local load sharing (LLS) scheme.

This is a mean-field model which ignores any fluctuation in local stress profile of the fibers.

- LLS scheme : In local load sharing (LLS) model, the stress of the ruptured fiber is equally distributed on the nearest neighboring intact fibers only.

Also there exists some intermediate redistribution scheme in the literature where the stress redistribution is neither mean field nor extreme localized. Example of such schemes in the literature are given below :

- A fraction $g$ of the the stress of the broken fiber is distributed locally and a fraction $1 - g$ is redistributed according to global load sharing scheme [74].
- The stress of broken fiber is redistributed as $r^{-\gamma}$ where $r$ is the distance between the broken fiber and the fiber that takes the extra load. $\gamma$ is the decay parameter [75].
- Only $R$ surviving neighbors of the broken fiber carries the extra load [76].

After such redistribution there might be further breaking of fibers due to local enhancement of stress profile. This redistribution might lead to global failure or stops when the stress acting on a fiber could not reach the next threshold limit. At this situation the applied stress is increased to break the next weakest link and the

process continues until all fibers break. The last stress that is applied to the model before global failure is known as the critical stress ($\sigma_c$) of the model.

# Chapter 3

# Effect of Disorder

In this chapter, we have explored the effect of disorder in a statistical mechanical model of fracture, namely the fiber bundle model. Disorder is introduced in the model as fluctuation in threshold stresses of the fibers. Threshold stresses of the fibers are chosen randomly from a distribution of width $\delta$. $\delta$ is the measure of strength of the disorder in the model. We have studied the model by varying $\delta$ .

## 3.1 Brittle to quasi-brittle transition in fiber bundle model

Temperature, pressure and porosity have an indirect effect on disorder in the model, which in turn cause brittle to quasi-brittle/ductile transition. Here we have directly tuned the disorder in the fiber bundle model and want to see weather such transition exists with disorder or not.

### 3.1.1 Equal load sharing scheme

In equal load sharing scheme (described in previous chapter) we have studied how the model goes from brittle like abrupt failure scenario to continuous failure scenario by tuning the disorder $\delta$. At low values of $\delta$, the failure of the system occurs, typically, from the rupturing of a single fiber, the fiber with minimum breaking threshold $x_{min}$. On the other hand, for large values of $\delta$, failure occurs through a series of stable states at different stress levels. As the applied load is raised, the system goes through these states in succession of avalanches of rupturing of fibers till the critical stress $\sigma_c$, when the remaining fraction $n_c$ of fibers ruptures bringing failure of the entire system.

We ask the following questions, (i) is there a critical value $\delta_c$ demarcating these two regimes: brittle and quasi-brittle , (ii) what are the features of the transition at $\delta_c$ and (iii) what are the manifestations of the transition on the macroscopic properties of the model. Lastly, the possible relevance of these features to brittle to quasi-brittle transition observed in real materials is discussed.

Here, we present results for uniform distribution of $\Phi(x) = 1/2\delta$ over the window $a$ to $(a + 2\delta)$ within the range [0,1]. For uniform distribution, the existence of a $\delta_c$ has been mentioned before [77, 78]. In ref [78] a general expression of $\delta_c$ was derived for different threshold distributions. Our analytical calculation gives $\delta_c = a/2$, in accordance with [78]. For $\delta \leq \delta_c$, there is a finite probability $P_b$ that rupturing of the weakest fiber leads to the failure of the entire system. $P_b \to 0$ as $\delta \to \delta_c^-$. At $\delta_c, P_b \sim L^{-\eta}$, with $\eta \approx 1/3$, where $L$ is the size of the system. We further show analytically that, as $\delta$ approaches $\delta_c$, the relaxation time $\tau$ diverges as $\tau \sim |\delta - \delta_c|^{-1}$. Our numerical analysis gives the finite size scaling form of the relaxation time. At $\delta_c$, the evolution of fracture becomes extremely slow. We observe that the failure of the system occurs in succession of avalanches of rupturing of fibers with time. The avalanche size distribution $P(s)$ shows a scale free behavior and follows: $P(s) \sim s^{-\kappa}$

with $\kappa \approx 1/2$. These exponent values suggest that the critical behavior at $\delta_c$ is in a new universality class. $\delta_c$ is the transition point which demarcates brittle phase (for $\delta < \delta_c$) from the quasi-brittle phase (for $\delta > \delta_c$) in the model.

**Analytical results**

The analytical calculation is based on finding the number of surviving fibers at each stable phases of the model at different stress levels. At an applied stress $\sigma_{ext}$, the fraction of unbroken fibers is obtained by integrating the probability distribution $\Phi(x)$ from minimum of the distribution $a$ to the redistributed stress $\sigma_r$. If $U^*$ is the fraction unbroken then the redistributed stress will be given by $\sigma_r = \sigma_{ext}/U^*$. Then fraction unbroken is

$$\begin{aligned} U^* &= \int_a^{\sigma_{ext}/U^*} \Phi(x)dx = \int_a^{\sigma_{ext}/U^*} \frac{1}{2\delta}dx \\ &= \frac{1}{2\delta}\left(\frac{\sigma_{ext}}{U^*} - a\right) \end{aligned} \tag{3.1}$$

Above expression will give a quadratic equation of $U^*$ whose solution is

$$U^* = \frac{1}{2}\left(1 + \frac{a}{2\delta}\right) \pm \frac{1}{2}\left[\left(1 + \frac{a}{2\delta}\right)^2 - \frac{4\sigma_{ext}}{2\delta}\right]^{1/2}. \tag{3.2}$$

At the point of failure, above equation admits only one solution. This will be satisfied only if the term under the root vanishes. This gives the critical stress $\sigma_c$ and critical fraction $U_c$ of the fibers at the failure point:

$$\sigma_c = \frac{2\delta}{4}\left(1 + \frac{a}{2\delta}\right)^2 \quad \& \quad U_c = \frac{1}{2}\left(1 + \frac{a}{2\delta}\right). \tag{3.3}$$

If we start from a high $\delta$ value and keep it lowering, $U_c$ will increase and reaches 1 at $\delta = \delta_c$. On further lowering of $\delta$ value, $U_c$ will remain at unity. In the region $\delta < \delta_c$, the analytical solutions are not valid. Inserting $U_c = 1$ in Eq.3.3, we get the critical

value $\delta_c$ below which the model shows abrupt brittle like fracture in thermodynamic limit: $\delta_c = a/2$. If $a$ is 0, the abrupt fracture will never occur in the model and the system will always break in steps with increasing external stress. On the other hand if $a > 0.5$, the fracture will always be abrupt.

From the dynamics of the system, at the external stress $\sigma_{ext}$, the fraction $U(t+1)$ of the unbroken fibers at time step $(t+1)$ can be expressed in terms of the fraction $U(t)$ at time $t$ [79]. At any time $t$, if $U(t)$ is the fraction unbroken, then the redistributed stress at that time will be $\sigma_t = \dfrac{\sigma_{ext}}{U(t)}$. Fraction unbroken at the next time step will be

$$U(t+1) = 1 - P(\sigma_t) = 1 - P(\sigma_{ext}/U(t)) \tag{3.4}$$

where $P(\sigma_t)$ is the probability of surviving fibers at stress $\sigma_t$. For uniform distribution, inserting this value of $P(\sigma_{ext}/U(t))$ we get the expression for fraction unbroken at time $t+1$, disorder $\delta$ and applied stress $\sigma_{ext}$:

$$U(t+1, \sigma_{ext}, \delta) = \frac{1}{(2\delta)} \left[ a + 2\delta - \frac{\sigma_{ext}}{U(t, \sigma_{ext}, \delta)} \right]. \tag{3.5}$$

The rate of change of $U(t, \sigma_{ext}, \delta)$ is given by : $dU(t, \sigma_{ext}, \delta)/dt = U(t+1, \sigma_{ext}, \delta) - U(t, \sigma_{ext}, \delta)$. Combining this with Eq.3.5 we get

$$\frac{dU(t, \sigma_{ext}, \delta)}{dt} = -\frac{(2\delta)U^2(t, \sigma_{ext}, \delta) - (a + 2\delta)U(t, \sigma_{ext}, \delta) + \sigma_{ext}}{(2\delta)U^2(t, \sigma_{ext}, \delta)} \tag{3.6}$$

We solve the above equation for a slight deviation $\Delta U$ of $U(t, \sigma_{ext}, \delta)$ from the breakdown point $U_c$ $(= U(t, \sigma_c, \delta))$: $U(t, \sigma_{ext}, \delta) = U_c + \Delta U$ $(\Delta U \to 0)$. Neglecting higher order of $\Delta U$ we get $U(t, \sigma_{ext}, \delta)^2 = U_c^2 + 2U_c\Delta U$. Substituting this in Eq.3.6 and assuming $U_c = 1$ at $\delta_c$, we can write

$$\frac{d\Delta U}{\Delta U} = -\frac{2\delta - a}{2\delta} dt = -\frac{1}{\tau} dt \tag{3.7}$$

Where $\tau$ is the relaxation time. Integrating Eq.3.7, we get the change in fraction of unbroken bonds: $\Delta U = Ae^{-t/\tau}$, where $A$ is a constant. Here, relaxation time has the form

$$\frac{1}{\tau} = \frac{2\delta - a}{2\delta} = 1 - \frac{a}{2\delta} \tag{3.8}$$

$$or, \tau \sim (\delta - \delta_c)^{-1}, \quad (\text{since } \delta_c = a/2) \tag{3.9}$$

Above behavior of $\tau$ clearly shows that the relaxation time diverges as $\delta \to \delta_c$.

To get better insight of the nature of the transition, we have studied the transition numerically. For simplicity, we have considered uniform distribution $\Phi(x)$ of half width $\delta$ and mean at 0.5. For such distribution $\delta_c = 1/6$ (obtained from analytical calculation). Numerical results are obtained on averaging over $10^4$ configurations and for system sizes ranging from $10^2$ to $10^6$.

**Response of the model to external stress**

Figure 3.1 shows $U^*$ for different values of applied stress $\sigma_{ext}$ and $\delta$. Here, the black region denotes the system after complete failure ($U^* = 0$) and yellow region represents the initial condition where all fibers are intact ($U^* = 1$). The color gradient is the partially broken phase ($0 < U^* < 1$). $\sigma_{ext}$ at the boundary of the black and yellow region denotes the critical stress $\sigma_c$. For $\delta < \delta_c$, $\sigma_c$ follows a straight line given by $a = 0.5 - \delta$. This is the region where we go from the yellow to black region by a single jump once the stress reaches the minimum threshold $a$ of the fibers. For $\delta > \delta_c$ the critical stress deviates from the straight line and approaches to $\sigma_c = 0.25$ at $\delta = 0.5$. In this region, fracture evolves through a series of partially broken stable states at different levels of applied load.

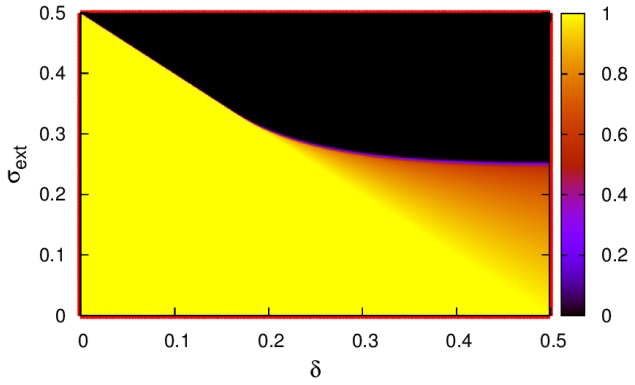


Figure 3.1: Fraction of unbroken bonds $U^*$ is plotted for different $\sigma_{ext}$ and $\delta$. In yellow region $U^* = 1$, while in the black region $U^* = 0$. The color gradient corresponds to partially broken configurations ($0 < U^* < 1$). At low $\delta$ values, the system goes from yellow to black region at a critical stress with an abrupt fracture. For $\delta > \delta_c$, the system goes from yellow to black region through a color gradient region signifying gradual fracture at different stress levels. The boundary of black region gives us the critical stress $\sigma_c$ for the system.

**Probability of abrupt failure**

Due to the finite size of the system, even below $\delta_c$, global failure (rupture of all the fibers in the system) is not always obtained starting from the rupture of the weakest fiber. We determine $P_b$, the probability of global failure starting from the rupture of the weakest fiber, for various $\delta$ values and for various system sizes (see fig.3.2). For a particular system size $L$, we define the critical $\delta$-value $\delta_c(L)$ at which $P_b$ goes to zero. It is quite clear that $\delta_c(L)$ has a system size dependence and approaches to $\delta_c$ as $L \to \infty$. We find that $\delta_c(L)$ satisfies the finite-size scaling relation:

$$\delta_c(L) = \delta_c + bL^{-\eta}, \tag{3.10}$$

where the exponent $\eta$ has a value $0.33 \pm 0.02$ and $b$ is a constant. The error bar is determined from the least square data fitting. It is to be noted that the fluctuation $\Delta U_c$ in the number of surviving fibers at the critical stress has been shown to scale as $\Delta U_c \sim L^{-1/3}$ [67, 80, 81]. It is this fluctuation in $U_c$, which determines the fluctuation in critical $\delta$-values for finite-size systems. This fluctuation should also

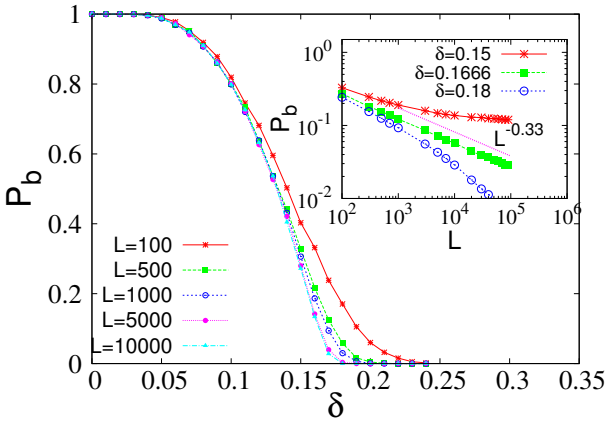


Figure 3.2: Plot of $P_b$ with $\delta$ for increasing system size values $L = 100$(star), 500(square), 1000(open circles), 5000(filled circles) and $10,000$(tringle). For low $\delta$, $P_b$ is close to 1. As $\delta$ increases, $P_b$ decreases till it goes to zero. This fall becomes more and more sharper as the system size is increased. In the inset variation of $P_b$ with system size $L$ is shown for $\delta = 0.15$(star), 0.1666(square) and 0.18(open circle). For $\delta = 0.15$, $P_b$ saturates, so that there is always a non-zero $P_b$ value. For $\delta = 0.18$, $P_b$ falls to zero exponentially fast. At $\delta_c$, $P_b \sim L^{-\eta}$, with exponent $\eta \approx 1/3$.

tell us the probability $P_b$ in a system of finite size.

Fig.3.2 (inset) presents the variation of $P_b$ with system sizes in the neighborhood of $\delta_c$. For $\delta < \delta_c$, $P_b$ tends to saturate and there is always a non-zero probability of rupturing of all the fibers starting from the single most vulnerable one. On the other hand, for $\delta > \delta_c$, $P_b$ falls off sharply to zero and probability of having an abrupt fracture vanishes in the thermodynamic limit ($L \to \infty$). At critical disorder $P_b$ shows a scale free behavior: $P_b \sim L^{-\eta}$, where $\eta = 1/3$.

### Divergence of relaxation time

To establish the critical behavior of at $\delta_c$, we study the relaxation time of the bundle at different $\delta$ values with system sizes ranging from $10^4$ to $10^5$. To determine relaxation time, we apply the minimum load that is needed to rupture the weakest fiber and the system is allowed to evolve (keeping the load constant) till it fails or reaches a stable state with partially broken bonds. Relaxation time is determined as the number of times the load is to be redistributed among the unbroken fibers

over the evolution of the system. At a particular $\delta$ value, for $10^3$ configurations the maximum of this relaxation times is determined. Again over $10^3$ configurations the average of this maximum values are obtained. We denote this average value as $\tau$ and use it to explain the critical behavior at $\delta_c$. Fig.3.3 shows this variation of $\tau$ with $\delta$ for different system sizes ranging from $10^4$ to $10^5$. Previous studies have dealt with the behavior of relaxation time close to critical stress [80, 82]. Here we have fixed the stress to be the minimum one and approaches critical point by tuning $\delta$ value.

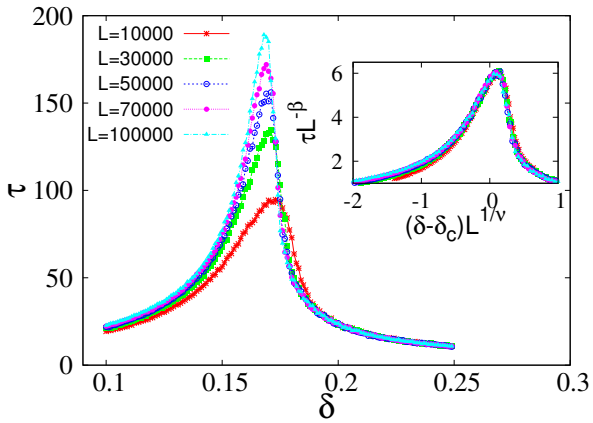


Figure 3.3: Relaxation time $\tau$ is plotted with $\delta$ for system sizes $L = 10000$(star), 30000(square), 50000(hollow circle), 70000(filled circle) and 100000(triangle). In the inset the scaling of $\tau$ is shown. The scaling is done by plotting $\tau L^{-\beta}$ against $(\delta - \delta_c)L^{1/\nu}$ for the above mentioned $L$ values with $\beta = 0.33 \pm 0.02$.

$\tau$ shows a maximum at $\delta = \delta_c(L)$ for system size $L$. As $L$ increases, the maximum value increases and the increment becomes sharper and sharper. Below $\delta_c$ the system experiences an abrupt failure within a few redistributing time steps starting from the rupture of the weakest fiber. On the other hand, for $\delta > \delta_c$, due to a wide range of threshold values, the minimum stress corresponding to the weakest fiber is not sufficient to break all the fibers in the system. Staring from some initial rupturing of the fibers, the system comes a stable configuration after few redistribution step for the stress. In both these cases, $\tau$ is finite. At $\delta = \delta_c$, $\tau$ diverges with system size

obeying a finite size scaling:

$$\tau \sim L^{\beta}\Psi\big((\delta - \delta_c)L^{\eta}\big), \tag{3.11}$$

where $\beta = 0.33 \pm 0.02$. The scaling function $\Psi(x)$ assumes constant value for $x = 0$ and for large $x$. Accordingly, at $\delta_c$, $\tau \sim L^{\beta}$, and close to $\delta_c$,

$$\tau \sim (\delta - \delta_c)^{-\gamma}, \tag{3.12}$$

where $\gamma = \beta/\eta = 1$. The scaled $\tau$ is shown in the inset of fig.3.3. The scaling is sensitive to the choice of the value of the exponent $\beta$, which determines the error bar of it by simply checking the collapse in the scaling. The value of the exponent $\gamma = 1$ is in agreement with our analytical result.

**Avalanche size distribution**

The definition of avalanche that we have adopted is quite different from the conventional one. The avalanche in our case is calculated in between two redistributing steps in stead of two stress increment. Figure 3.4 shows the avalanche size distribution $P(s)$ verses the avalanche sizes $s$. We start from applying a low load on the system, sufficient enough to rupture only the weakest fiber. Once a fiber is ruptured, the stress is redistributed among the remaining unbroken fibers. The breaking of fibers between any two consecutive stress redistribution steps constitute an avalanche and the number of fibers broken gives the size of the avalanche. For $\delta < \delta_c$, the distribution tends to level off (up to a certain avalanche size) showing big avalanches are equally probable. In this region, after few big avalanches, the system fails completely within few time steps. In the region $\delta > \delta_c$, the distribution falls off very fast showing that, in this region, the system ceases to evolve after few small avalanches starting from the rupturing of the weakest fiber. At $\delta = \delta_c$ the

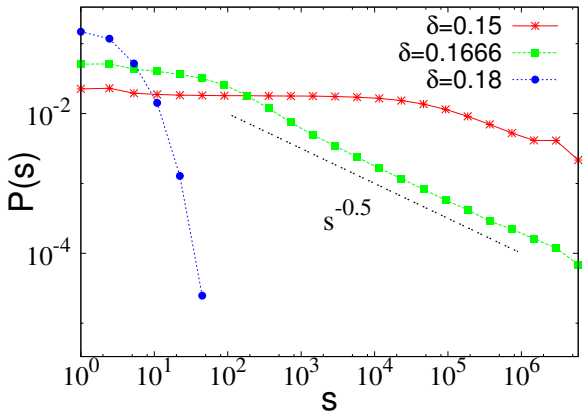


Figure 3.4: $P(s)$ vs. $s$ is plotted for $\delta = 0.15$(star), 0.1666(square) and 0.18(filled circle). For $\delta < \delta_c$, the distribution levels off. Since in this region the avalanches are uncorrelated there is always a probability of having an avalanche of any size (even as big as the system size). For $\delta > \delta_c$, $P(s)$ falls to zero exponentially fast and there is no big avalanches found. At $\delta = \delta_c$, $P(s)$ falls in a power law behavior with exponent $\kappa = 0.5 \pm 0.01$.

distribution is a power law:

$$P(s) \sim s^{-\kappa}, \tag{3.13}$$

where the exponent is given as $\kappa = 0.5 \pm 0.01$.

We have also checked this critical behavior for the truncated Gaussian and power law distribution of threshold of the fibers. Within the error bar, the exponent values suggest universality.

### 3.1.2 Local load sharing scheme

Both pure abrupt brittle response and non abrupt quasi-brittle response is present in local load sharing fiber bundle model, along with a particular disorder value (similar to $\delta_c$ in ELS scheme) separating this two regions. Due to local stress concentration in LLS scheme this particular disorder value neither has critical behavior nor uniqueness. We denote this disorder as $\delta_L$, since it changes with system size. A detailed discussion of the crossover from brittle region to quasi-brittle region for LLS scheme is discussed below.

**System size dependent brittle to quasi-brittle response**

To characterize the brittle and quasi-brittle region, first of all we have observed the abruptness in failure process at different disorder values. For that purpose we have studied fraction of unbroken bonds, $U_c$, just before global failure. $U_c = 1$ suggests a brittle like abrupt failure. For $U_c < 1$ the model shows a continuous failure like quasi-brittle response. With decreasing disorder value $U_c$ starts approaching unity. For a constant system size, the disorder at which $U_c = 1$ is noted and that is the $\delta_L$ corresponding to size $L$.

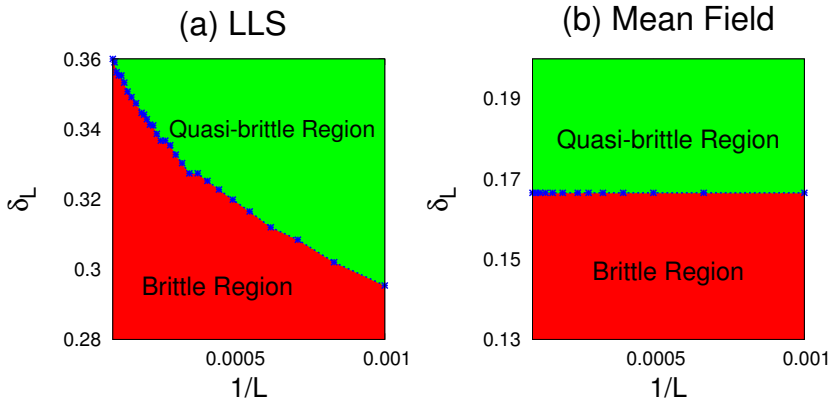


Figure 3.5: (a) Variation of brittle and quasi-brittle region with system size ($L$) for the most local load sharing scheme. Brittle region increases with increasing system size.
(b) System size independent brittle and quasi-brittle region in mean field case. The division of the regions happens around $\delta_c = 1/6$.

Figure 3.5 shows the variation of $\delta_L$ with increasing system size. In mean field limit (Fig. 3.5b) there is no system size effect on $\delta_L$ ($\delta_L = \delta_c = 1/6$) and hence we get constant amount of brittle region ($\delta < 1/6$) and quasi-brittle region ($\delta \geq 1/6$) at any $L$ value. In case of LLS scheme (Fig. 3.5a), $\delta_L$ increases as we go to higher and higher system size. This intern increases the brittle region and the fracture becomes more and more abrupt. Finally in thermodynamic limit (towards the origin of figure 3.5b) the failure is always brittle like abrupt.

**Approaching thermodynamic limit with increasing system size**

We have already seen that there is a clear signature of system size effect on $\delta_L$ and therefore on the abruptness of fracture in LLS model. At any certain disorder we can define a particular system size $L^*$ above which $U_c$ approaches 1.0 (numerically the tolerance is taken as: $L = L^*$ if $(1.0 - U_c) < 10^{-3}$) and the failure process is always abrupt. This study is carried out for disorder ranging from 0 to 0.5. We observe

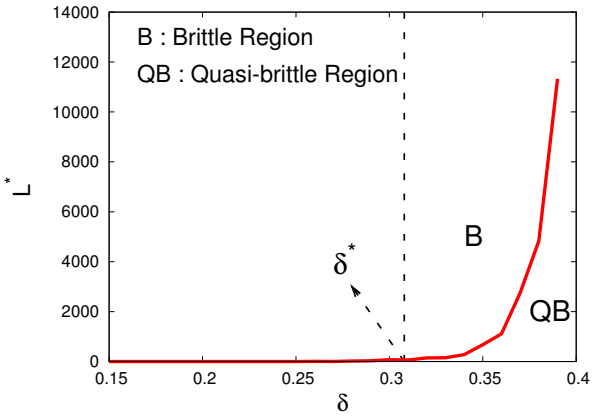


Figure 3.6: $L^*$ is the system size above which the fracture is purely abrupt. Variation of $L^*$ with disorder for LLS scheme. Below $\delta = \delta^*$ the fracture is always abrupt and its really easy to achieve . This is the pure brittle region. For $\delta > \delta^*$ there is a certain region below $L^*$ where the failure is quasi-brittle like non abrupt.

that (Fig.3.6) there is a disorder value $\delta^*$ exists below which $L^*$ is very small and its very easy to achieve brittle failure. This is the brittle failure dominated region in the model. Beyond $\delta^*$, $L^*$ increases very fast and there is a certain region below $L^*$ where the failure process is quasi-brittle like non abrupt. In this region the failure can be both brittle (B) and quasi-brittle (QB) depending on the system size.

## 3.2 Size effect of responses in fiber bundle model

In the introduction part we have already discussed the effect of notch or micro-crack present in the real system that leads to weakest link of a chain concept [13, 14, 15], according to which the fracture in presence of many defects is determined primarily

by the most vulnerable defect and that is how the idea of extreme statistics is applied to fracture. Quasi-brittle materials indeed show a large scatter in fracture strength, the distribution of which can be represented by the long-tailed Weibull distribution. The distribution is a telltale signature of the underlying extreme events that controls triggering of fracture. The distribution suggests power law fall of the fracture strength with system size $L$ ($\sigma_c \sim 1/L$), which is readily seen in experiments [83, 84, 85]. Apart from long-tailed Weibull distribution, experiments in different materials also shows Gumbell distribution where in-stead of power law $\sigma_c$ falls as inverse logarithmically ($\sim 1/\log L$) [24]. Whether the fracture strength should follow Weibull or Gumbell distribution is a matter of debate for long time. We have studied this distributions for failure stress and its system size dependence in fiber bundle model with both equal and local load sharing scheme.

### 3.2.1 Equal load sharing scheme

For equal load sharing fiber bundle model, as described in chapter 2, after rupture of every fiber the stress is redistributed equally among all other surviving fibers. This is basically the mean field limit of the model, where fluctuation in local stress profile of the fibers are neglected. There is no local stress concentration observed in the neighborhood of the broken fibers. Due to this behavior system size effect is not seen in equal load sharing fiber bundle model. Parameters like: strength of the model, abruptness in failure process, avalanche size distribution, divergence of relaxation time at critical stress, does not change when we change the sample size. Though the picture in LLS scheme very different from the mean field picture.

### 3.2.2 Local load sharing scheme

Due to over simplification in stress redistribution rule in case of mean field fiber bundle model, the system size effect is not possible to capture. To understand the effect of system size on fracture strength we have adopted local load sharing (LLS) fiber bundle model where the only surviving neighbors of a broken fiber caries the extra load (see description of the model in chapter 2).

#### System size effect on strength and failure abruptness

Figure 3.7 shows the behavior of critical stress ($\sigma_c$) with a continuous variation of disorder ($\delta$). Results are produced for system sizes up to $5 \times 10^4$ with $10^4$ configurations. The dotted line (not the vertical ones) in the figure gives the locus of

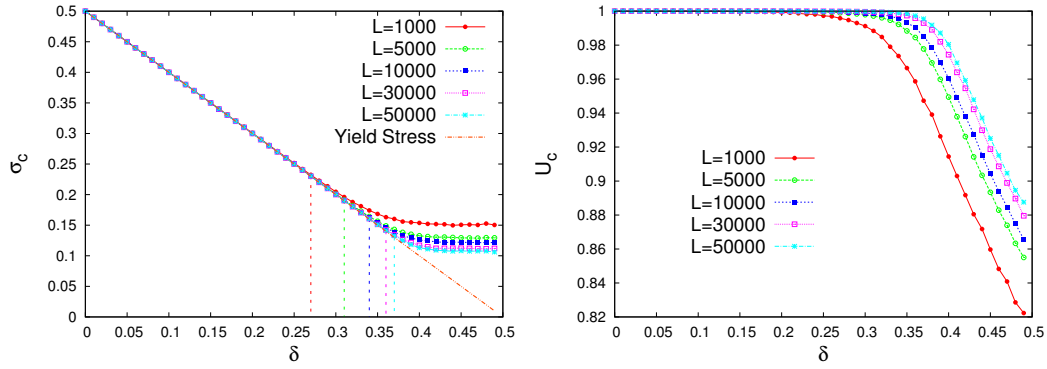


Figure 3.7: Left figure: Study of $\sigma_c$ with continuous variation of disorder value ($\delta$). Results are generated for system sizes ranging from $10^3$ to $5 \times 10^4$. Dotted line gives the yield stress ($\sigma_y$), the separation of elastic and plastic region. $\delta_L$ is the disorder below which we get brittle failure. $\delta_L$ increases with increasing $L$ values.
Right figure: $U_c$ is studied with LLS scheme for different system sizes ($10^3 \geq L \geq 5 \times 10^4$) with increasing $\delta$ values. The value of $\delta_L$ below which $U_c = 1$ is the disorder value separating brittle region from the quasi-brittle one. Increase in system size shows increase in $U_c$ value and hence leads the model to higher abruptness.

yield stress ($\sigma_y$), that separates the linear elastic region from the plastic region in the response curve. For brittle response $\sigma_c$ and $\sigma_y$ coincides with each other since there is almost zero plastic region in the response curve. Vertical dotted lines give the values of a particular disorder, $\delta_L$, above which critical and yield stress deviates

from each other. $\delta_L$ for different system sizes are different and continuously increases as we go to higher $L$ values. On the other hand in mean field limit (ELS scheme) $\delta_L = \delta_c = 1/6$ independent of system size.

**Effect of disorder on $L$ dependence of $\sigma_c$**

The system size effect of critical stress ($\sigma_c$) is already known to behave as $1/\log L$ [24, 86, 87, 88, 89, 90, 91] when the threshold strength of the fibers are distributed over (0:1). But on the contrast at very low $\delta$ value, due to the brittle like failure, the critical stress is basically the the minimum strength corresponding to the weakest link of chain. In that limit the minimum threshold as well as $\sigma_c$ should scale as $1/L$ with increasing system sizes. One of the previous work [92] shows this $1/L$ behavior at very low disorder. In spite of above studies a proper understanding of change in behavior of $\sigma_c$, from inverse logarithmic (high $\delta$) to scale free behavior (low $\delta$), is still absent. Here the behavior of $\sigma_c$ is studied throughout all $\delta$ region and the above change in behavior is characterized. This behavior is quite similar to the study of the distribution of nominal stress, seen in real systems [93, 94, 95, 96]. One early paper has already discussed about the fact which distribution, Weibull or normal, is appropriate for nominal stress in real specimens [97].

Figure 3.8 shows the change of $\sigma_c - \sigma_l$ with increasing $L$ values separately for logarithmic (lower) and scale free (upper) behavior. $\sigma_l$ is the lower limit of the uniform distribution. Lower figure shows that for high disorder region ($0.4 < \delta < 0.5$) $\sigma_c - \sigma_l$ gives a straight line when plotted against $1/\log L$. As we go to lower $\delta$ values the behavior deviates from the straight line behavior. On the other hand in upper figure $\sigma_c - \sigma_l$ is plotted with $L$ in log scale.In lower disorder ($0 < \delta < 0.3$) it gives a straight line with slope $-1$. This is the $1/L$ behavior we have discussed earlier [74]. This slope decreases rapidly within the window $0.3 < \delta < 0.4$ and saturates at a low value ($\approx 0.2$) beyond $\delta = 0.4$. To understand the accuracy at

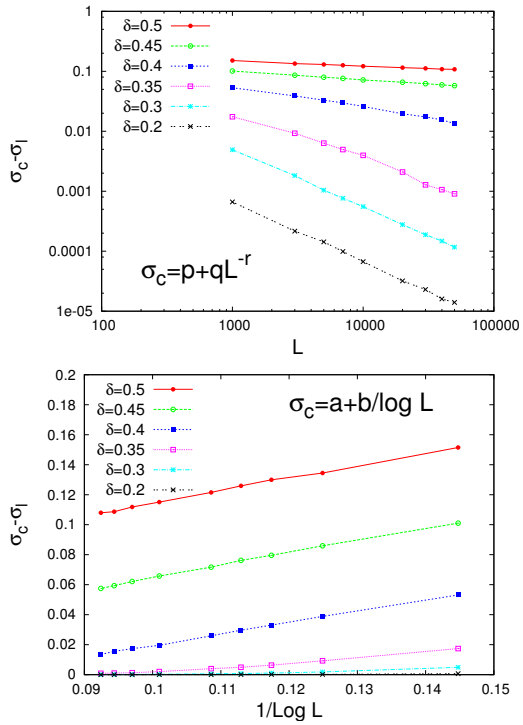


Figure 3.8: Lower: $\sigma_c - \sigma_l$ is plotted against $1/\log L$ at different $\delta$ values. Clearly the data gives a straight line for higher disorder ($0.4 < \delta < 0.5$) and at that region the logarithmic behavior matches with numerical data with less error. At low disorder it deviates from the line.
Upper: $\sigma_c - \sigma_l$ is plotted against $L$ in log scale. For low disorder it shows a scale free behavior with slope $-1$. Above $\delta = 0.35$ this slope changes rapidly and saturates to very low value ($\approx 0.2$) and the system size effect becomes very weak. Here the logarithmic behavior is more appropriate.

which the numerical data fits with logarithmic and power law behavior the best fit condition is obtained with following functions :

$$\text{(i) } f(x) = p + qL^{-r} \qquad \text{and}$$

$$\text{(ii) } g(x) = a + \frac{b}{\log L}.$$

Figure 3.9 gives the best fit of $f(x)$ and $g(x)$ with the numerical data for $\delta = 0.5$, 0.4, 0.35, 0.3, 0.2 and 0.1. Both $a$ and $p$ converges to $\sigma_l$ as the model reaches the thermodynamic limit. Figure 3.9 shows that for low $\delta$ values $f(x)$ matches much well with the simulated data than $g(x)$. If we go to higher disorder ($\delta > 0.4$) then fluctuation of the simulated data from both the functions are very small and both functions seem to fit well. This probably happens because at high disorder the power ($r$) of scale free fit becomes very small. We know that $x^\alpha$ with low $\alpha$ value acts as $\log x$. Because of this in high $\delta$ value its difficult to distinguish between logarithmic and scale free nature.

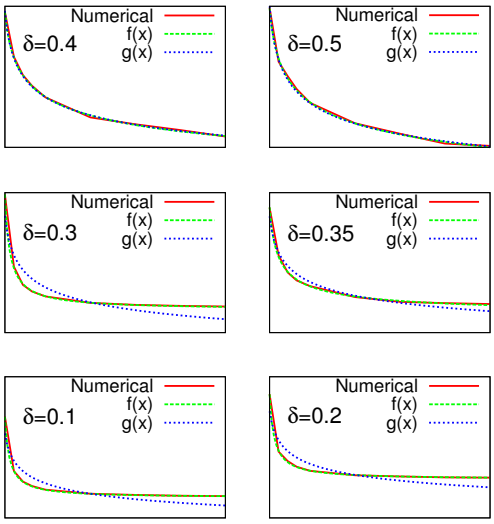


Figure 3.9: Numerical data for system size effect of critical stress is fitted with $f(x) = p + qL^{-r}$ (power law behavior) and $g(x) = a + b/\log L$ (logarithmic behavior). The fitting is done for $\delta = 0.1$, 0.2, 0.3, 0.35, 0.4 and 0.5. For high disorder ($\delta > 0.4$) value both $f(x)$ and $g(x)$ matches with the data with less error. At low disorder ($\delta < 0.3$) the power law behavior matches much accurately than the logarithmic one.

**Transition from scale free to logarithmic behavior**

Figure 3.10 shows the quantitative behavior of the exponents $r$ and $b$ with increasing disorder. Change in this two exponents mainly occur within the disorder window

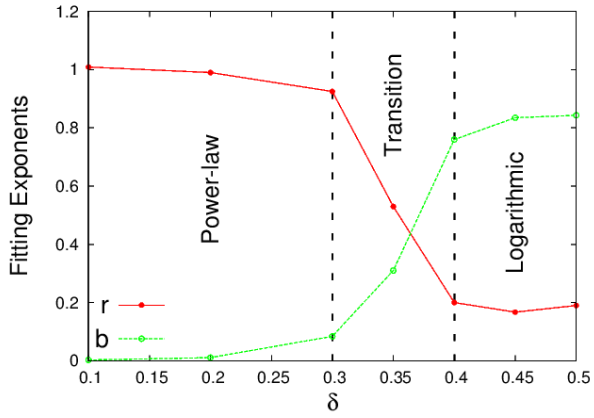


Figure 3.10: The exponents from figure 3.8 ($r$ and $b$) are shown with a continuous variation of disorder. Both $r$ and $b$ remains at a same value for $\delta > 0.4$ as well as $\delta < 0.3$. Within the region $0.3 < \delta < 0.4$ these exponents shows abrupt changes. This is the transition region where the simulated data shifts from power law to logarithmic behavior.

$0.3 \leq \delta \leq 0.4$. Below 0.3 strength of the model falls in a scale free behavior with increasing system size, while beyond 0.4 it matches with inverse logarithmic behavior.

## 3.3 Study of failure time

Above signature of critical disorder value $\delta_c$, in ELS scheme, can also be captured from the study of failure time of the model. Time to fracture, $\tau_f$, at a particular load, often used to determine the reliability and strength of the material, is an outcome of this spatial and temporal micro cracking dynamics. It is defined to be the time taken for the system to fracture under a certain loading condition. Basically, failure time is the relaxation time (see section 3.1.1) when a critical stress is applied to the model.

### 3.3.1 Equal load sharing scheme

The failure time is studied numerically in equal load sharing scheme. Mainly we have observed the distribution for failure time and its system size effect and different disorder (both $\delta > \delta_c$ and $\delta < \delta_c$).

#### Analytical result

Analytically the difference in brittle and quasi-brittle region is, for $\delta > \delta_c$ we have analytical expression for $\sigma_c$ and $U_c$ (Eq.3.3). While in region $\delta < \delta_c$, $\sigma_c$ is the minimum threshold of the chain and $U_c$ is simply 1. Due to abrupt failure in brittle region ($\delta < \delta_c$), we have $\sigma_c = a + \epsilon$, where $a$ is the minimum of the distribution. $\epsilon$ is the term that takes care of the system size effect in the bundle. As we go to higher system size $\epsilon$ value decreases as the threshold of the weakest link comes closer to $\sigma_l$. The recursion relation of Eq. 3.5 this case takes the form

$$U(t+1, \sigma_c, \delta) = 1 + A\left(1 - \frac{1}{U(t, \sigma_c, \delta)}\right) - \frac{\epsilon}{2\delta U(t, \sigma_c, \delta)} \tag{3.14}$$

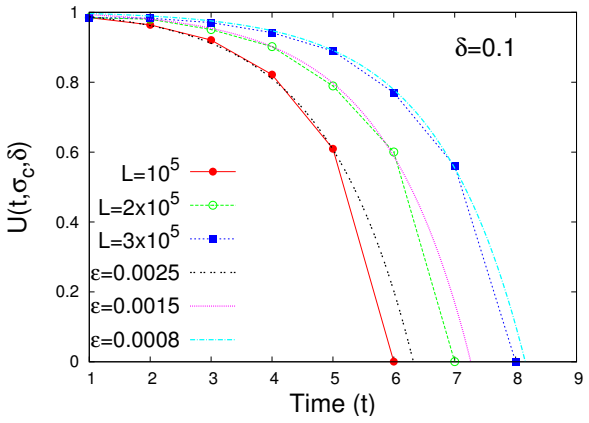


Figure 3.11: Study of $U(t, \sigma_c, \delta)$ with increasing time steps for system sizes $10^5$, $2 \times 10^5$ and $3 \times 10^5$. Disorder is kept fixed at $\delta = 0.1$. The black dotted lines show the analytical behavior according to Eq. 3.16 with $\epsilon = 0.0025$, $\epsilon = 0.0015$ and $\epsilon = 0.0008$ respectively. The envelop of the curve increases as well as $\epsilon$ decreases as we go to higher system sizes.

where $A = \frac{a}{2\delta}$. As $U(0, \sigma_c, \delta) = 1$ its easy to see that $U(1, \sigma_c, \delta) = \left(1 - \frac{\epsilon}{2\delta}\right)$. Repeating this recursively, we get

$$U(t, \sigma_c, \delta) = 1 - \frac{\epsilon}{(2\delta - \epsilon)} \frac{1 - A^t}{1 - A} \tag{3.15}$$

In above expression the higher order of $\epsilon$ is neglected. Using the expression of $A$ we get

$$U(t, \sigma_c, \delta) = 1 - \frac{4\delta\epsilon}{(2\delta - \epsilon)(6\delta - 1)} \left[1 - \left(\frac{(1 - 2\delta)}{4\delta}\right)^t\right] \tag{3.16}$$

In figure 3.11 we have compared the analytical expression of $U(t, \sigma_c, \delta)$ with the numerical behavior. As higher order terms are neglected, the analytical result does not tally with the numerical findings at large times. We will discuss this behavior later in this chapter while discussing the numerical results.

### Distribution for failure time

The failure time $\tau_f$ is the envelop of the $U(t, \sigma_c, \delta)$ vs $t$ curve. We have determined it numerically for different $\delta$ values. Numerically $\tau_f$ is estimated as the number of redistributing steps through which the bundle evolves before global failure when a critical stress is applied on it. In this paper, the results are shown for uniform distribution of half width $\delta$ and mean 0.5 to assign individual thresholds of the

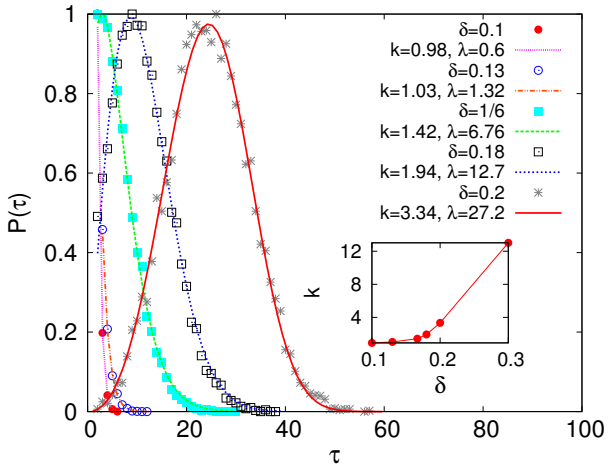


Figure 3.12: The distribution for failure time for different $\delta$ is fitted with Weibull distribution with shape parameter $k$ and scale parameter $\lambda$. The numerical results are fitted with various $k$ and $\lambda$ values. In the inset the variation of shape parameter $k$ is shown with $\delta$.

fibers.

Figure 3.12 shows the distribution $P(\tau)$ of failure times $\tau$ at different $\delta$ values for system size $L = 10^4$. $P(\tau)$ follows the Weibull distribution: $P(\tau) = \left(\frac{k}{\lambda}\right)\left(\frac{\tau}{\lambda}\right)^{k-1} e^{-\left(\frac{\tau}{\lambda}\right)^k}$, where $k$ and $\lambda$ are respectively the shape and scale parameter of the distribution. Larger the $\delta$ the distribution becomes wider. The Weibull distribution of failure times in heterogeneous materials has been discussed before [98, 99].

### System size effect of failure time

Figure 3.13 shows the system size effect of the average failure time ($\tau_f = \langle\tau\rangle$) at different disorder values. $\tau_f \sim L^\alpha$ for all $\delta$ with $\alpha$ as the exponent of the power law. Above $\delta_c$, $\alpha$ shows an universal behavior and remain constant independent of $\delta$. In vanishingly small disorder the model is bound to fail in redistributing step independent of system size. As the model approaches this vanishingly small disorder limit ($\delta \to 0$) the exponent $\alpha$ decreases. $\tau_f$ satisfies the following scaling behavior:

$$\tau_f \sim L^\alpha \begin{cases} \alpha = 1/3, & \delta \geq \delta_c \\ \alpha = \Phi_-(\delta), & \delta < \delta_c \end{cases} \tag{3.17}$$

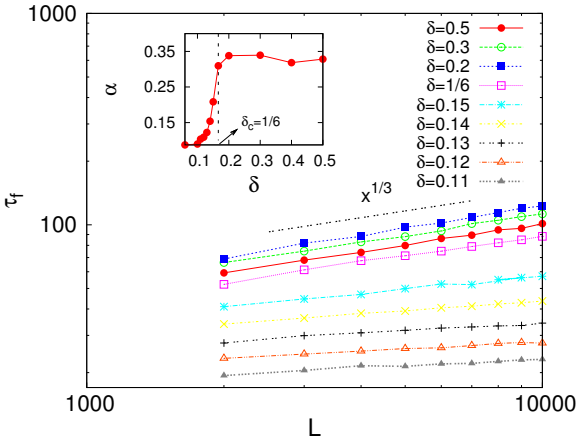


Figure 3.13: System size effect of maximum average relaxation time $\tau_f$ at different $\delta$ value. $\tau_f$ shows a scale free behavior with system size $(L)$ : $\tau_f \sim L^{\alpha}$. Value of exponent $\alpha$ remains constant at $1/3$ for $\delta > \delta_c$, while it keeps decreasing below $\delta_c$ and the system size effect of $\tau_f$ gradually vanishes.
Inset: Variation of scaling exponent $\alpha$ with varying disorder value. For $\delta > \delta_c$, $\alpha$ saturates at a value $1/3$. Below $\delta_c$ the exponent value decreases as we go to lower $\delta$ values.

where $\Phi_{-}(\delta)$ decreases with decreasing disorder values. For uniform threshold distribution with $\delta = \frac{1}{2}$, the relaxation time at critical stress has been found before to diverge as $L^{1/3}$ [80]. At $\delta_c = \frac{1}{6}$, the relaxation time also diverges as $L^{1/3}$ [100].

### 3.3.2 Local load sharing scheme

For local load sharing scheme the behavior of relaxation time is quite different.

- The distribution of $\tau_f$ is also a Weibull distribution at different disorder values.
- The system size effect on $\tau_f$ is very different from equal load sharing scheme. Here we do not find any signature of the disorder value separating abrupt and non abrupt failure. At all disorder values: $\tau_f \sim L$.

## 3.4 Conclusion

- For equal load sharing fiber bundle model we get a brittle to quasi-brittle like transition at a critical disorder value $\delta_c$. Below $\delta_c$ the failuire is abrupt and model gives linear response only. Beyond $\delta_c$ the model fails continuously through a number of stable states.

- System size effect of critical stress ($\sigma_c$) and abruptness in failure is seen for local load sharing scheme. At high disorder $\sigma_c$ goes as $1/\log L$, whish was observer earlier in fiber bundle model. At low disorder the critical stress rather falls in scale free manner ($\sim 1/L$). We obtain a intermediate window of disorder value where this transition/crossover of behavior takes place.

# Chapter 4

# Effect of Stress Release Range

The effect of disorder on the failure mode has been discussed in previous chapter. In this chapter will be discussing the effect of stress release range on fracture. Using random fuse model as a simple prototype of the disordered solid, it has been shown [101] that for finite disorder, the failure mode of the system, in the large system size limit, is always nucleation driven and therefore abrupt. The stress is nucleated around the largest defect and the defect grows in size until the the system fails. The precursory events (scale free size distribution of rupture events prior to failure etc.), previously seen in the model [102], were attributed to the transient effect, implying these would not lead to the final fracture in the large system size limit. The only exception is the limit of extreme disorder [103]. However, experimentally such precursory features are observed (see e.g., [104]) for which the extreme disorder is not necessarily the physical condition.

In this chapter, we ask the question: how the range of stress relief zone affects the mode of fracture in disordered solids? This range is an intrinsic property of the solid that depends on its elastic constants. We study fiber bundle model as a prototype of disordered solids and show that if the range $R$, over which the stress is released in unit time following a local rupture, is sufficiently large then the system

shows scale-invariant precursory behaviour that survives even in the large system size limit. In particular, we find that if $R$ scales slower than a cut-off scale $R_c \sim L^{\zeta}$, with $\zeta = 2/3$, where $L$ is the system size, the failure mode is nucleation dominated. On the other hand, if $R$ scales faster than $R_c$, the failure properties are dominated by the mean field behaviour even in the $L \to \infty$ limit and with finite disorder. In this case, local fiber ruptures are uncorrelated in space and the final failure is preceded by precursory avalanches, of rupturing fibers, of all sizes. $\zeta$ can be identified with the inverse of correlation length exponent. We apply the criterion to fiber bundle model with power-law stress redistribution [105] and find the value of the exponent in the power law that demarcates the two limits. This demarcation is also supported by simulation results.

It is known that in one extreme limit of the model, where the failure of one element affects the stability of all others equally, the failure mode is precursor driven and the damage is diffused in the system in the sense that it occurs all over the system in an uncorrelated manner. In another limit, where the failure of one element affects only the element(s) nearest to it, the failure is nucleation driven [91, 106]. Both these situations are, however, away from reality. The first case implies the absence of any notion of distance in the system, hence excluding the concept of stress nucleation altogether. The second limit indicates a very low elastic modulus, which is also physically unrealistic. There have been previous attempts [105, 107, 108, 109] to interpolate between these two extreme limits of the model, but they did not arrive at any general criterion for which the crossover is observed.

## 4.1 Stress release range $R$ in fiber bundle model

We take here a linear array of fibers and set a redistribution rule for the load of a failed fiber such that the range over which the stress is redistributed has a scale

$R$. We follow the rule, whereby, the load on a broken fiber is distributed uniformly among the $R$ successive surviving fibers (see also [110]) on either side of the broken fiber. The system is loaded gradually until it fails completely. The disorder is modelled by random failure thresholds of the fibers, which are drawn from a uniform distribution in $[0:1]$. In one scan of the lattice (one time step), all fibers having load more than their thresholds are broken. The load of these fibers are redistributed according to the redistribution rule mentioned above. If the load on any one of these neighbors exceeds threshold after redistribution, it is broken in the next scan. This continues until no fiber is broken in a given scan. The external load is then increased just upto the point when the weakest of the remaining surviving fiber breaks and the above dynamics is continued.

## 4.2 Extreme limits of $R$

Consider the case when $R$ is constant, i.e. it does not scale with the system size $L$. This is a generalization of the usually studied local load sharing model ($R = 1$). For threshold distributions that extend to zero (e.g., uniform distribution in $[0:1]$), for an arbitrarily small applied load $\sigma$, there will be a large enough patch of length $m$ of successive broken fibers, such that the redistributed stress on its surviving neighbours ($R$ on either sides) will exceed the maximum threshold value (1 in this case) [64] leading to the catastrophic failure of the system. It was shown that for $R = 1$, $\sigma_c \sim 1/\ln L$ [64] where $\sigma_c$ is the critical value of stress for which the system fails. For arbitrary $R$, one would expect $m \sim R$. But as long as $R$ does not scale with $L$, the qualitative behaviour is found (numerically) to remain the same.

A more interesting case is when the $R$ is varied to see the effect on the failure mode. Obviously, for $R \sim L$, the load redistribution becomes global by definition and the mode of failure is expected to be gradual with usual avalanche statistics.

The question we intend to answer is: Does the scaling of the effective range have to be as fast as linear to lead to global load sharing failure mode?

### 4.2.1 Cluster density

A signature of the global load sharing process is the uncorrelated failure of fibers when load is increased. This leads to creation of new broken patches in the system with the increase of load. On the other hand, onset of nucleation is essentially the growth of one patch that engulfs all other patches, leading to the failure of the system. An effective way to detect nucleation, therefore, is to monitor the number

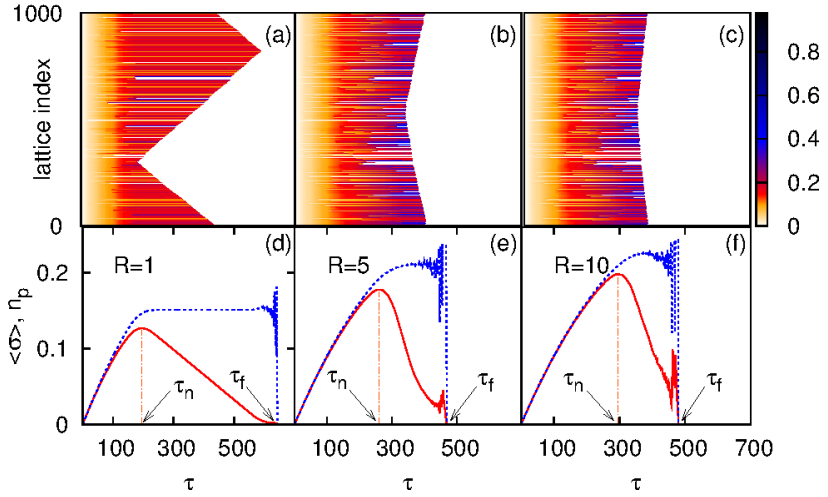


Figure 4.1: The upper panel shows the variation of the stresses on the fibers in the system with redistribution steps $\tau$. The onset of nucleation can be seen from the tip of the cone, beyond which one broken patch grows and the total number of patch starts decreasing. The onset time gets shifted to a higher value as the stress redistribution range $R$ is increased ((a)-(c)) and expected to merge with failure time in the global load sharing limit. The panel below ((d)-(f)) shows the variation of average stress per fiber ($\langle\sigma\rangle$; denoted by dotted lines) and number ($n_p$) of patches (denoted by solid lines), scaled by system size, for corresponding $R$ values. The onset of nucleation ($\tau_n$) is the point where the number of patch starts decreasing and the stress per fiber saturates (at the critical value) until failure point ($\tau_f$) is reached.

of broken patches in the system. The top panel of Fig. 4.1 shows the evolution of the load per fiber with time (defined here as the number of load redistribution

step). As can be seen from Fig. 4.1 (a)-(c), for different values of $R$, upto the onset of nucleation (tip of the cone), each fiber carries almost the same load. When nucleation sets in, one single patch starts growing leading to the complete failure of the system. As can be seen from the bottom panel, the time $\tau_n$ of onset of nucleation is where the number of patches (scaled by system size) starts decreasing. It is also the time when the load per fiber value becomes constant (implying that to be the critical load). After many steps of load redistribution (each redistribution considered here as one time step), the system finally fails completely at time $\tau_f$.

### 4.2.2 Nucleation time

As the range of load sharing is increased, the nucleation and failure times approach each other i.e., $\Delta\tau = \tau_f - \tau_n$ decreases (see figure 4.1). While the order of these events can not be reversed, they may come very close (up to a scale of critical relaxation time in mean field limit) as $R$ increases, implying vanishing of the nucleation mechanism. In Fig. 4.2 (inset) the variation of the time interval $\Delta\tau$ is shown with $R$ for different system sizes. It shows a initial linear decrease, followed by a saturation regime, which can be interpreted as the vanishing of nucleation mechanism. The value of the saturation time depends on the system size. Repeating the study of $\Delta\tau$ for different system sizes we find an overall scaling form

$$\Delta\tau \sim L^{\alpha}\mathcal{F}\left(\frac{R}{L^{\zeta}}\right). \tag{4.1}$$

Satisfactory data collapse is obtained for $\alpha = 0.33 \pm 0.01$ and $\zeta = 0.66 \pm 0.01$ (see Fig. 4.2), which leads to the conjectured exact values as $\alpha = 1/3$ and $\zeta = 2/3$. The scaling function $\mathcal{F}(x)$ has the form $\mathcal{F}(x) \sim 1/x$ for $x < 1$ and $\mathcal{F}(x)$ becomes constant for $x \geq 1$.

Before interpretation of the consequences of such scaling form, let us try to

understand the exponent values. For small values of $R$, the nucleation sets in from the weakest patch, where the rest of the system is almost intact. The patch then grows, breaking $2R$ neighbors on each step of redistribution, until the whole system breaks. The time required for complete failure should be $\Delta\tau \sim L/v_f$, where $v_f$ is the growth velocity of the fatal patch and it has to cover almost the entire lattice, hence the numerator $L$. Now, as $\sim 2R$ fibers break in each step, $v_f \propto R$, giving $\Delta\tau \sim L/R$. This is what is seen in the early part of the scaling. Now, the part where $\Delta\tau$ is independent of $R$, the failure mode is of global load sharing type, where the relaxation time at the failure point diverges as $\Delta\tau \sim L^\alpha$, with $\alpha = 1/3$ [80]. Therefore, for matching of the two scaling forms at the crossover one must have $L^\alpha(R/L^\zeta)^{-1} \sim L/R$, giving $\alpha + \zeta = 1$. Therefore, $\zeta = 2/3$ as is also seen from data collapse.

In brittle region since there are no stable states, the failure time (see chapter 3, section 3.3) and $\Delta\tau$ is same. Now from the study of failure time we get $\tau_f$(or $\Delta\tau$) $\sim L^\alpha$, where $\alpha$ is constant for $\delta > \delta_c$ and increases with $\delta$ in the region $\delta < \delta_c$. Combining this result with $\Delta\tau \sim L/R$ at $R = R_c$, we get: $R_c \sim L^{1-\alpha}$.

To understand the physical picture, let us consider the probability distribution of stress values within the system. For a global load sharing model each fiber carry same stress, hence the distribution function is a delta function. On the other hand, for stress nucleation (and failure driven by it), the stress distribution function must have a finite width that survives the large system size limit. The width depends on the (i) the range $R$ of the stress release in unit time (the width is narrower as $R$ becomes larger) and (ii) the fluctuation in the number of broken fibers, which contributes in the increase of the width. The functional dependence of the width is expected to be of the form $\Delta\sigma \sim \Delta N/R$, where $\Delta N$ is the fluctuation in the number of surviving fibers. Since we are approaching the mean field critical point, the relevant fluctuation is the one seen near it. But it is known that the fluctuation in the

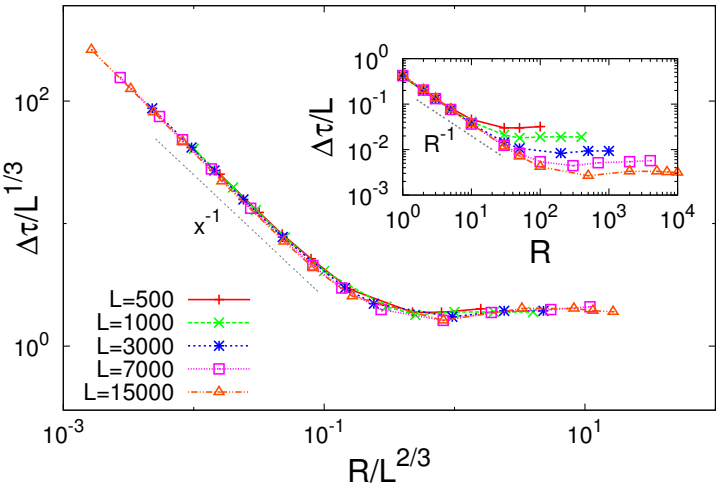


Figure 4.2: The data collapse for the time difference $\Delta\tau = \tau_f - \tau_n$ for different system sizes $L$ and for different range $R$ as given by the scaling form Eq. (4.1). The inverse decay marks the nucleation regime, which stops when $R \sim L^{2/3}$ and global load sharing region begins. In this regime, $\Delta\tau$ becomes $R$ independent but depends on $L$ (as can be seen from the inset). The initial collapsed region in the inset confirms the dependence $\Delta\tau \sim L/R$ in the nucleation regime, and the lines spreads out as soon as global mode starts dominating.

fraction of surviving fibers (over the disorder configurations) scales as $\Delta U_c \sim L^{-1/3}$ [108, 111], thus the fluctuation in the number will scale as $\Delta N \sim L^{2/3}$. Therefore $\Delta\sigma \sim L^{2/3}/R$. Hence $\Delta\sigma$ retains a finite value in the large system size limit only when $R = R_c \sim L^{2/3}$ (which is seen from the scaling relation Eq. (4.1)). For $R > R_c$, the stress distribution is narrow, which corroborates to the absence of stress nucleation. This sets the scaling criterion for nucleation.

### 4.2.3 Avalanche size distribution

The phrase 'large system size limit' is very important in the context of the scaling of $R_c$, since for a given choice of $(R, L)$ the system may show scale free avalanche distribution, which may go away for large system size $L > R^{3/2}$ when the fracture mode becomes nucleation dominated. As can be seen from Fig. 4.3 (a), when the system size is small, for a given $R$, $\tau_n$ and $\tau_f$ are very close. In that region, the

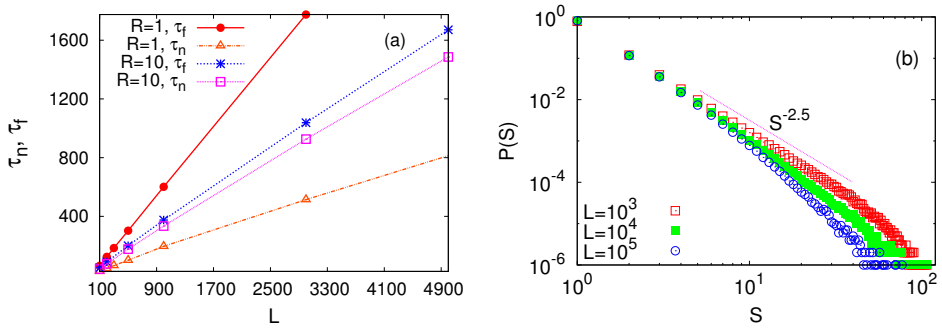


Figure 4.3: The top figure (a) shows the variation of the onset time for nucleation $\tau_n$ and failure time $\tau_f$ with system size $L$ for two values of $R$. For small system sizes and bigger $R$ value, the two times are very close to each other. In this region, mean-field 'critical behavior' can be observed. For fixed $R$ value, this 'criticality' will not survive in the large system size limit. The figure at the bottom (b) shows the avalanche size distribution for fixed $R$ value (100) while the system size is increased. For $L = 10^3$, the ratio $R/L^{2/3} = 1$, putting the system in the critical regime where $P(S) \sim S^{-2.5}$. But for $L = 10^4$ and $L = 10^5$ the ratio becomes $\approx 0.215$ and $\approx 0.046$ respectively. The avalanche size distribution in the last two cases deviates from the above scale free distribution.

avalanche size distribution (Fig. 4.3 (b)) and other related quantities shows mean field behavior. But as the system size is increased, the critical behavior goes away. This is similar to the 'finite size criticality' mentioned in Ref. [101]. However, in our case we can tune the range of stress release and the mean-field like critical behavior survives in the thermodynamic limit provided the range $R$ increases sufficiently fast (although sub linearly) with system size.

## 4.3 Scale free stress redistribution scheme

We expect that the scaling given by Eq. 4.1 is valid for other forms of load redistribution where one has a characteristic length scale. We have checked this for several cases such as exponential decay, linear decay etc. of stress redistribution. An interesting question is what happens for a 'scale free' redistribution rule, e.g power-law redistribution? In this case, the load redistributed on the $j$-th fiber after the failure of $i$-th fiber is proportional to $1/|i-j|^{\gamma}$ [105]. The distribution is not truly scale

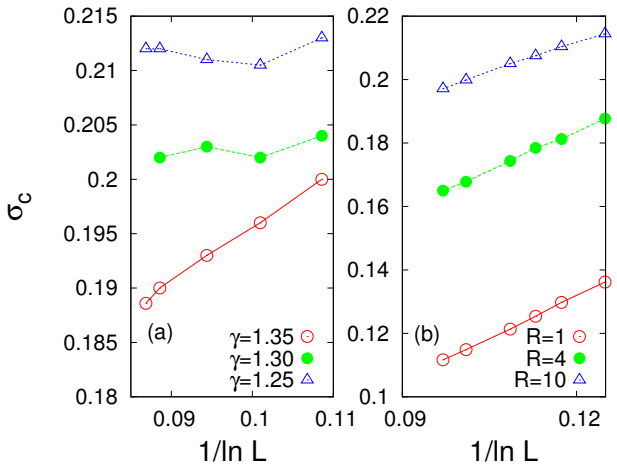


Figure 4.4: The left figure (a) shows that the failure threshold $\sigma_c$ goes to zero with $1/\ln L$ when $\gamma < \gamma_c = 4/3$ in the case of power-law load redistribution, showing the validity of the proposed scaling criterion that the effective range must scale faster than $L^{2/3}$ (or $\gamma < 4/3$) for global load sharing mode. The inverse logarithmic decay is similar to what is observed for uniform load sharing within range $R$ for $R < L^{2/3} < 1$ (b).

free, because it has two cut-offs, viz the lower cut-off due to lattice spacing (which we take as unity) and a upper cut-off due to finite system size.

### 4.3.1 One dimension

A quantity 'average range of interaction' will interpolate between two extremities, ELS and LLS scheme, as $\gamma$ is tuned. Remembering the normalization $A\int_1^L dx/x^\gamma =$ constant, one can always calculate the average (effective) length of interaction as $R^{eff} = \langle x \rangle \sim \frac{1-\gamma}{2-\gamma}\frac{L^{2-\gamma}-1}{L^{1-\gamma}-1}$. Clearly for $\gamma < 1$, $R^{eff} \sim L$ for large $L$. Also, $R^{eff} \to$ constant for $\gamma > 2$ implying nucleation scenario with fixed ranged interaction. But for $1 < \gamma < 2$, $R^{eff} \sim L^{2-\gamma}$ for $L \to \infty$. According to the scaling argument presented above, the critical value of the exponent $\gamma_c$ for which the failure behavior crosses over from nucleation to global load sharing mode is to be given by $2 - \gamma_c = 2/3$ or $\gamma_c = 4/3$. In support of this claim, in Fig. 4.4 we have shown the behavior of critical load $\sigma_c$ for fracture for various $\gamma$ values. It is seen that for $\gamma > \gamma_c = 4/3$, $\sigma_c \sim 1/\ln L$, which is similar to what we see in the nucleation regime for uniform load redistribution among $R$ neighbors with $R/L^{2/3} \to 0$ as $L \to \infty$. On the other hand, $\sigma_c$ saturates to a non-zero value when $\gamma < 4/3$, as is expected in global load

sharing scheme.

### 4.3.2 Two dimension

In two-dimensions, to introduce the notion of range, we search along positive and negative $x$ and $y$ axes from the broken fiber and go up to a distance $x_+, x_-, y_+$ and $y_-$ until $R$ surviving neighbors are found. We then redistribute the load within the rectangular region $(x_+, y_+)$, $(x_-, y_+)$, $(x_-, y_-)$, $(x_+, y_-)$. Of course, there can be other choices, for example a circular region of radius $R$. While that could work well for higher values of $R$, but for smaller values there could be situations where there were no surviving fibers within that region. Moreover, such details are unlikely to affect the scaling behavior, which is also evident from the fact that our prediction matches well with power-law load redistribution studied in Ref. [105].

An important result is when we perform the same treatment system size effect of stress release range in two dimension: $R_c \sim L^b$ with $b < 1 (= 0.85)$. This has an interesting consequence when power-law load sharing is done. In this case, the fraction of load received by an intact fiber at a distance $r$ is proportional to $1/r^\gamma$ [105]. Here one can define an effective range as $R_{eff} = \langle r \rangle = \int_1^L rP(r)2\pi r dr = \frac{2-\gamma}{3-\gamma}\frac{L^{3-\gamma}-1}{L^{2-\gamma}-1}$, where $P(r) \sim 1/r^\gamma$. For $\gamma < 2$, $R_{eff} \sim L$, implying mean-field regime. Also, for $\gamma > 3$, $R_{eff} \sim const.$, therefore it is always local load sharing type. However, for $2 < \gamma < 3$, $R_{eff} \sim L^{3-\gamma}$ in the large system size limit. Since $R_c \sim L^b$, to get the crossover value for $\gamma$ we have to compare $R_{eff}(\gamma_c) \sim R_c$, giving $\gamma_c = 3 - b$. But $b < 1 (= 0.85)$, giving $\gamma_c > 2 (2.15)$. This explains an apparent result for $\gamma_c > 2$ [105], which can now be claimed with much more numerical accuracy.

## 4.4 Effect of range in spring ladder model

We have carried out this study with varying range to another model in fracture, the spring ladder model. We have already discussed spring network model in chapter 2. Spring ladder model is basically spring network model with following modifications:

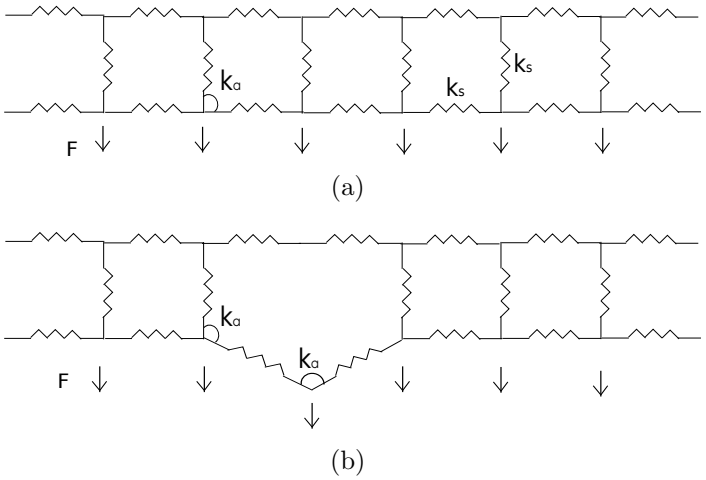


Figure 4.5: The spring ladder model with external force $F$ applied on the lower layer nodes (a) before breaking of a spring and (b) after breaking of a spring showing the deformed network.

1. The dimension of the bundle is $L \times 2$ instead of $L \times L$.

2. The horizontal springs have infinite threshold and hence not allowed to break on application of external stress. Only the vertical springs have random finite threshold.

3. Force is applied along $+ve$ and $-ve$ y-direction. Along $+ve$ and $-ve$ x-direction periodic boundary condition is applied.

Basically by replacing the the fibers in fiber bundle model with Hookean springs we can construct this spring ladder model. By using an angle potential between connected springs, the nature of redistribution can be localized or distributed depending on the stiffness of the angle potential. Here a ladder shaped spring network

is simulated under load control conditions. The results analyze the effect of varying load redistribution on the fracture characteristics. The different fracture modes exhibited by the model are analyzed.

The behavior of the system with varying angular elastic constant $k_\alpha$ is studied. Various characteristics of the system, as it evolves to a critical point, are analyzed. Comparing our results to the characteristics of ELS and LLS fiber bundle models we get the two extreme limits of the model with varying $k_\alpha$ values.

### 4.4.1 Simulation technique

The model is a spring ladder with two rows of horizontal springs connected by vertical springs at nodes as shown in Fig. 4.5. The number of vertical springs, L, denotes the size of the system. The springs are Hookean with the potential, $E_B = k_s \times (r_i - r_0)^2$. Here $r_0$ is the distance between two nodes connected by a spring, when no external force acts on the system. Initially all the springs are equally spaced with $r_0 = 1$. $r_i$ is the length of the spring $i$ at any given instant during the simulation. The force constant $k_s$ is equal to 0.1. The relative movement of springs connected at a given node is governed by an harmonic angle potential, $E_A = k_\alpha \times (\alpha - \alpha_0)^2$. At the initial configuration of the system, the angle between springs connected at a common node, $\alpha_0$ is at 90 degrees. The angle force constant $k_\alpha$, determines the extent of deflection between two springs for given conditions of loading. This parameter is the most crucial to the present study and its value is varied over a wide range, as will be detailed in the next section. The Hamiltonian of the system can hence be given by : $H = \frac{1}{2}\sum(k_s(r - r_0)^2 + k_\alpha(\alpha - \alpha_0)^2)$.

The system is loaded by adding a force with only a y-component, $F$ to every node on the lower layer. At every iteration, the resultant force $f_i$ at each node $i$ is estimated and the dynamics of the node is determined by solving $f_i = m_i a_i$

using the velocity varlet algorithm. The mass $m_i$ at node $i$ is taken as unity and $a_i$ is the acceleration. The integration time step $\delta t$ is fixed based on the maximum of the force carried by the nodes such that the value of $\delta t \times \max(f_i)$ is of the order of $10^{-4}$. The vertical springs are each assigned a random breaking threshold, uniformly distributed with width $\rho = 1.0$. A spring is assumed to break and removed from the system when the threshold is exceeded. The horizontal springs are not allowed to break during the course of the simulation and they act as the mode through which load transfer is effected in the network. The displacement of the nodes at the top layer in the y-direction is not allowed. Periodic conditions are used in the x-direction to account for boundary forces. To ensure quasi static loading conditions, the imposed external force is just enough to break the weakest spring. The system then evolves by redistributing the load among the remaining springs until the resultant force of the system in the x and y-direction is zero. In other words the system reaches equilibrium. As shown in Fig. 4.5(b), where a vertical spring has failed, the node in the bottom layer experiences force imbalance causing a deflection in the horizontal springs. The extent of this deflection is governed by the value of $k_\alpha$, which in turn governs the y-component of the force added to the neighboring nodes by the deflection. After the system reaches equilibrium, the applied force $F$, is incremented to cause the next failure. The failure of a single spring may lead to a cascade of breaks due to redistribution. The external force increments are continued till the system reaches a critical state beyond which the system evolves to complete failure with successive breaking springs.

### 4.4.2 Abruptness in failure process

The fraction of unbroken springs, $U_c$, at the critical point is estimated at different $k_\alpha$ values. In the LLS case, the weakest fiber breaking can lead to subsequent breaking of all the fibers, giving $U_c$=1. In the present study the average value of $U_c$ is given

in Fig. 4.6 at different $k_\alpha$ values. Three distinct regions can be observed. At low $k_\alpha$ values, where more localized load distribution is observed, the $U_c$ values exhibits an almost plateau value of 0.85. At the other extreme of high $k_\alpha$, another plateau like limit is reached at 0.55. In between these two regions, a transition region is observed. This transition from a nucleating to percolation behavior will be explored in detail below.

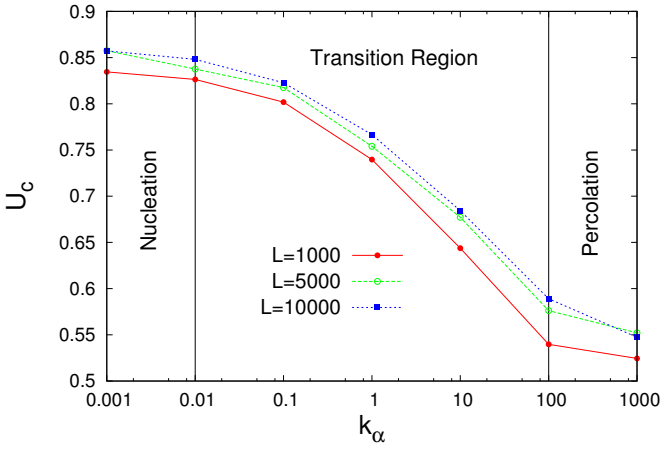


Figure 4.6: Variation of fraction of unbroken springs,just before the global failure, with $k_\alpha$ values for system sizes $10^3$, $5 \times 10^3$ and $10^4$. For low $k_\alpha$, $U_c$ is quite high and the failure process is abrupt. At high $k_\alpha$ values the result matches with the existing results of ELS fiber bundle model.

Analyzing the reasons behind the limiting plateau like behavior at both extremes, the following observations are made. With decreasing $k_\alpha$, once the maximum deflection that can be achieved near a broken fiber is reached any further decrease in $k_\alpha$ make no impact on localization. In the case of increasing $k_\alpha$ eventually ELS behavior is expected. But with deformation it is observed that instability sets in. This adds an imposed localized behavior on the system which prevents a pure ELS critical point. The instability phenomena can be avoided by imposing external conditions on the system. Though not addressed here, this would then lead to ELS value of 0.5. Another point to be noted is that the limiting values of 0.85 and 0.55 are variable when the width of the disorder distribution varies. The nature of deformation evolution, is determined by comparison with probability curve for random

breakage of fibrils [100].

### 4.4.3 Randomness in rupture event

Fig.4.7 shows the variation of patch density with fraction of broken springs. $U$ is the fraction unbroken. A patch is defined as broken spring accompanied by a unbroken one at its nearest neighbor. If we assume that the rupture of springs are random, then patch density will be given by $U(1-U)$. This is the random fracturing curve (inverted parabola) shown in figure 4.7. It is observed that at high values of $k_\alpha$, the random behavior curve is closely followed by patch density. In the case of low $k_\alpha$ ($\approx 0.001$), the system behavior deviates from the random curve even when very less fraction of the spring is broken. This indicates the onset of localized dynamics. For

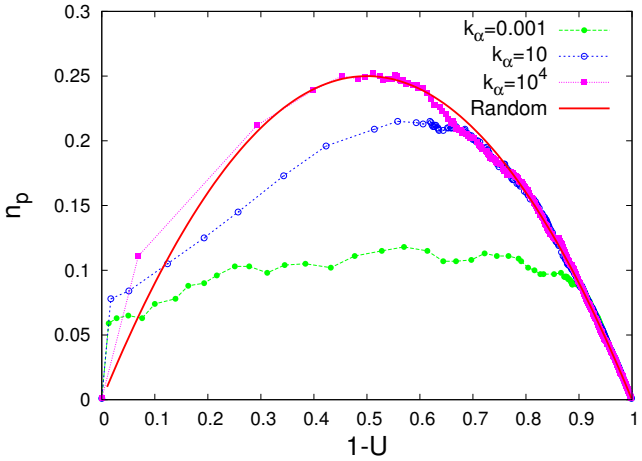


Figure 4.7: The number of clusters per site is plotted with increasing fraction of broken springs $(1-U)$, for $k_\alpha$ values $10^{-3}$, 10 and $10^4$. The behavior is compared with the random fratuaring event on a 1d chain.

low $k_\alpha$ value the number of clusters per site is constant even when the fraction broken increases. This indicates that the pre-existing clusters are growing in size. In the intermediate value of $k_\alpha = 10$, a combination of random breaks and localized breaks are observed with the deviation from random curve at a much higher fraction of broken fibers. Above study clearly shows that the deformation characteristics shifts from a nucleation dominated to percolation dominated with increase in $k_\alpha$.

### 4.4.4 Avalanche size distribution

An important characteristics of fracture process is the nature of avalanche size distribution of broken springs. While the equal load sharing model was analytically proven to exhibit a power law statistics with a exponent value of 2.5 [64], the local load sharing models were found to have a varying exponent value dependent of the strength distribution and the size of the sample. They found that for uniform distribution, a typical value of 4.2 - 5 was obtained from simulations of different sample sizes [87]. It would be of interest to study the effect of the load sharing methodology adopted in this work on avalanche distribution. The avalanche statistics at the limiting stages of nucleation and percolation exhibit exponent values of 4.8 and 2.5 respectively as seen in Fig 4.8. The value of 4.8 matches the value reported by Ref. [87]. The samples in the transition zone however depict a mixed response,

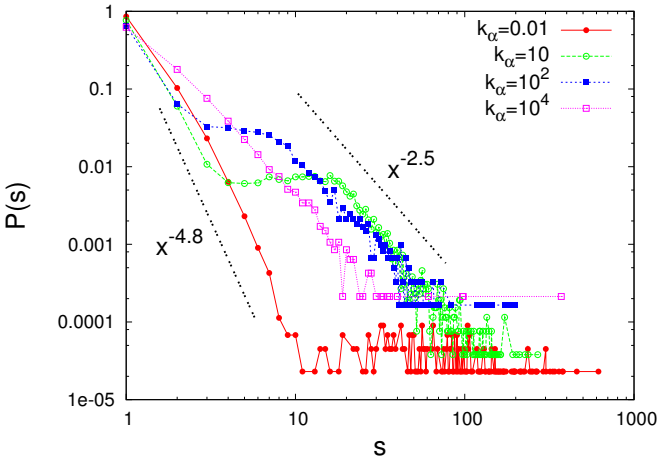


Figure 4.8: The avalanche size distribution at different $k_\alpha$ values. The exponent of the power law behavior is seen shifting from the ELS value of 2.5 to a LLS value of 4.8 as $k_\alpha$ decreases.

where the small size range follows LLS characteristics and the large size range follows ELS characteristics, with the intermediate size range exhibiting a flat profile with no power law behavior. As seen in Fig 4.8, as the value of $k_\alpha$ increases, the size ranges exhibiting LLS statistics and flat profile decrease in width. The size range exhibiting ELS statistics increases until at very high $k_\alpha$ complete ELS behavior is

observed. Thus the limiting cases of the model though not exactly having ELS and LLS university class values for the critical fiber fraction, exhibit the exponent values for avalanche distribution similar to ELS and LLS.

The effect of varying load redistribution is investigated in spring ladder model. The limiting cases for the system are identified as the fracture mode changes from nucleation dominated to percolation dominated. The characteristics of the system at the limiting case as well as at the intermediate states are studied using the avalanche size distribution. The exponents of avalanche distribution exhibit the same university class as that of ELS and LLS fiber bundle models at very high and low $k_\alpha$ values respectively. But at the limiting states the system only tends towards the these cases and does not replicate exactly.

## 4.5 Conclusion

- Fiber bundle model shows a transition from correlated/nucleating failure to uncorrelated/percolating failure around a critical range value $R_c$. This $R_c$ scales with system size as $\sim L^\zeta$. The value of $\zeta$ is 2/3 and 0.85 respectively for 1d and 2d fiber bundle model.

- Also spring ladder model shows a transition, from nucleation dominated to percolation dominated failure process, with variation of angular spring constant as an external parameter.

# Chapter 5

# Interplay of Stress Release Range and Disorder

We have already seen in previous chapters that disorder and stress release range has their effect in fracture process. In one hand, disorder takes care of the abruptness in failure process and on the other hand the stress release range deals with the rupture pattern: nucleating or percolation. At this point we can address the question : 'What will be the scenario if both the stress release range and disorder is tuned simultaneously ?'

In this chapter, we report a general phase diagram with the variation of stress release range and strength of disorder that captures all failure modes arising out of the interplay between those two parameters. In particular, we consider the fiber bundle model, which has been widely used as a generic model for disordered system over many years. With the help of the phase diagram we can now identify all its modes of failure, classify previous attempts to interpolate between some of those modes and most importantly arrive at scaling prescriptions in categorizing and predicting such failure modes.

## 5.1 Description of the model

Here we simulate the failure in fiber bundle model in one and two dimensions. Notion of the stress release range and disorder in fiber bundle model is already discusses in chapter 3 and chapter 4. Here we choose the failure thresholds of the fibers from a distribution of the form $p(x) \sim 1/x$ within a range $[10^{-\beta} : 10^{\beta}]$. For high values of $\beta$, the distribution becomes very broad, making the system a highly disordered one. Physically, this implies varying degree of impurities in the system, that can significantly influence its failure threshold. Following the failure of a fiber, should the load on it increase above its assigned threshold, the load is redistributed uniformly up to a distance $R$. We will first describe the phase diagram to explain its different phases. Subsequently we will discuss the methods of drawing the boundaries and relate them to previous results obtained in the model.

## 5.2 Description of the phases

Below, the description of all the phases are given with continuous variation of range $R$ and disorder $\delta$ is given. For low values of $R$ and $\beta$, we expect a nucleating failure, since the failure of a fiber will enhance the stress on its immediate neighbors. They will in turn become most likely to fail, because all fibers have failure thresholds close to each other. The initial damage will grow until the whole system collapses. So, in this limit the failure is both nucleating and brittle like abrupt. This damage nucleation can be prevented by either redistributing the load of a failed fiber in a relatively large distance, or by increasing the disorder such that the nearby fiber can have high failure threshold which compels distant fibers to fail first. Clearly, simultaneous effect of these two will bring the system to spatially uncorrelated failure even faster. When the disorder is small, all fibers have very similar failure threshold. Hence the failure of the weakest fiber will trigger an avalanche that will lead to failure

of the entire system. This brittle like failure mode is distinct from a quasi-brittle or ductile failure mode by the fact that in the latter cases the system goes through many stable states before it fails completely. The phases on $R - \beta$ plane that we

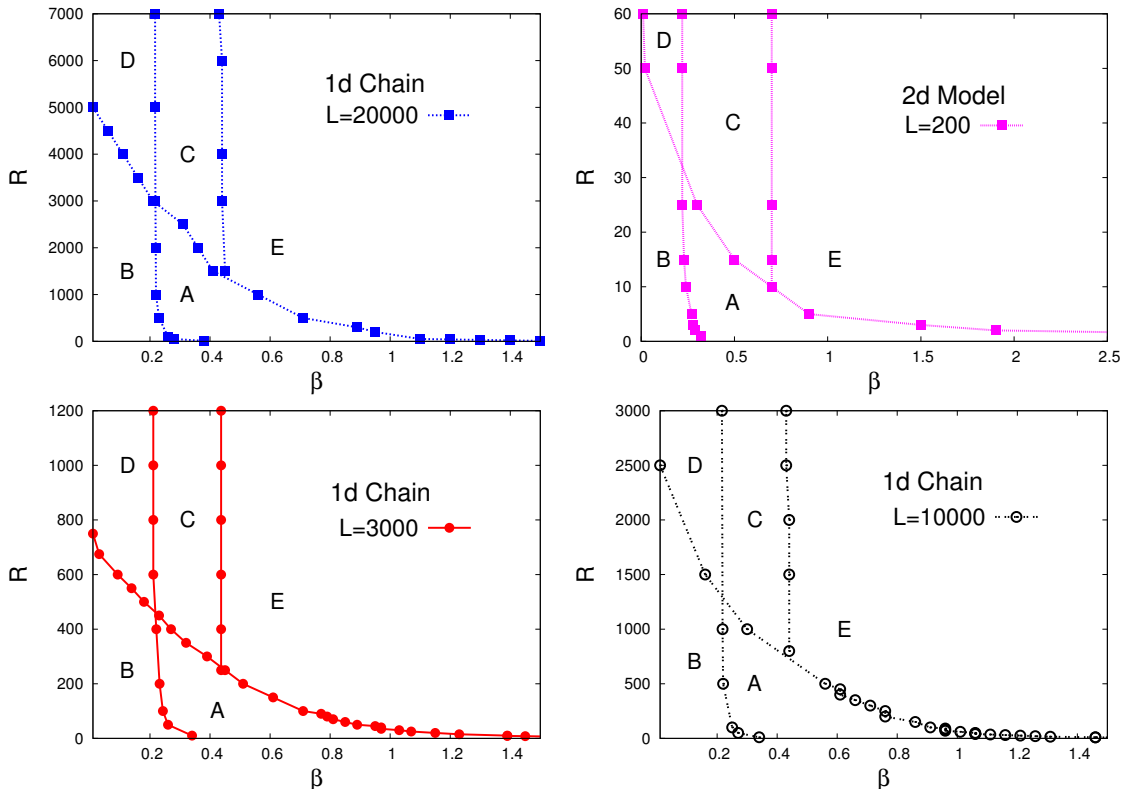


Figure 5.1: The figure shows all the regions on $R - \beta$ plane for 1d chain and 2d bundle. $B$ and $D$ are brittle region and shows abrupt failure. $A$ and $C$ shows quasi-brittle response. In region $A$ and $B$ the rupture process is correlated. In region $E$, there are no avalanches and the fracture process is percolation like random.

get with continuous variation of range and disorder is discussed below:

- **Brittle nucleating ($B$) :** This region falls in the low $R$ and low $\beta$ region. Due to low $\beta$, all the fibers have threshold values very close to each other. This basically increases number of redistribution and makes the failure process abrupt. On the other hand since range is also kept low, the stress can not redistribute very far from the broken fiber. As a result, after redistribution, the next failure is expected to happen from the neighborhood of the broken one. Failure process in this region is both nucleating and abrupt.

- **Brittle percolating ($D$) :** At low disorder and high range the failure is still abrupt but loses the correlation in rupture process. The fibers break randomly but without any precursory event. During the failure process it only gives a avalanche equals to the system size when a minimum stress corresponding to the weakest link is applied on it.

- **Quasi-brittle nucleating ($A$) :** We get this region for low $R$ but intermediate disorder value. Due to increment in disorder the thresholds of the fibers become distant to each other and we have to increase the external stress to break the bundle. The model goes through a number of stable states prior to complete failure. Though, the model breaks through a series of stable states, the rupture events are still correlated and bundle breaks through a nucleating crack.

- **Quasi-brittle percolating ($C$) :** We observe this region at intermediate disorder and high range value. The rupture process is random here. Also a continuous external triggering of applied stress is required to break the model. Only in this region the model shows scale free avalanche distribution with exponent $-5/2$. This is the mean field limit of the model which has been explored the most in the literature.

- **High disorder regime ($E$) :** We get this region at very high disorder value. In this region the failure is always random no matter what the range value is. Also the failure process is non-abrupt and only guided by external stress increment. As a result no avalanches are seen in this region.

Basically the failure processes in these above mentioned regions are combination of abrupt/non-abrupt as well as correlated/uncorrelated failure.

## 5.3 Study of the phase boundaries

Above we have already discussed the failure processes and there properties in different regions on $R-\beta$ plane. In this section we will discuss the criteria and numerical approaches through which the boundaries of these regions are drawn.

### 5.3.1 Boundary between nucleating and percolating failure

In the phase diagram, the region $A$ and $B$ together shows correlated rupture process and the failure is nucleating. On the other hand in region $D$, $C$ and $E$ the fracture process is percolating. The boundary, we are interested in, separates the region $A+B$ from region $C+D+E$. To draw the boundary between the region of correlated and uncorrelated failure process, we looked at spatial correlation in terms of number of clusters, $n_p$, formed by broken fibers. In one dimension, the number of clusters of broken fibers is simply the number of side by side broken and unbroken fibers present. For two dimension, we compare our results with 2d random site percolation problem [112].

#### Study of patch density

If $U$ is the fraction of surviving fibers at any point, then for complete random failure, the number of side by side broken and unbroken fiber will be $U(1-U)$ (normalized by system size). Any deviation from this inverted parabolic shape would then indicate spatial correlation. We measure the difference of the areas under the curves and when that disappears we can conclude that the spatial correlation has vanished. As discussed before, for high $R$ and $\beta$ values the spatial correlation will vanish. For intermediate disorder it is known [76] that the crossover to random failure takes place when $R_c \sim L^{2/3}$. That result is confirmed from this result as well. But for very low (scaling is non-universal [113]) and very high disorders (always uncorrelated) the

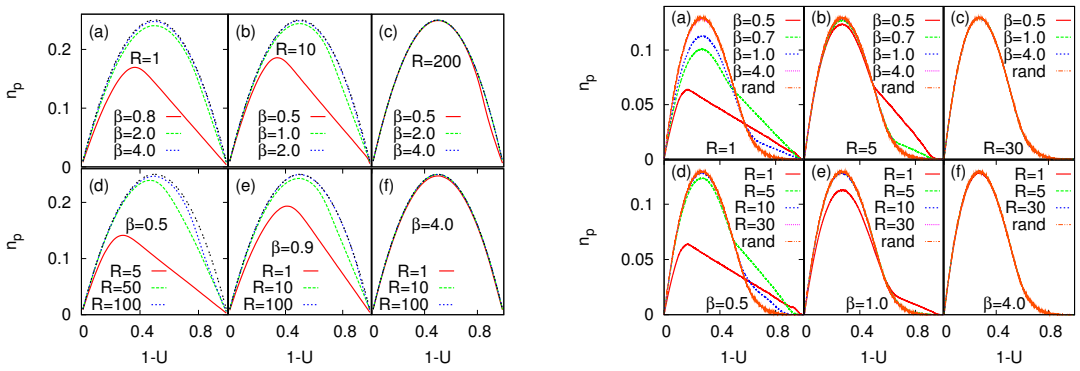


Figure 5.2: The variations of density of patch $n_p$ are shown for (a-c) constant range and different strength of disorder ($\beta$) and for (d-f) constant strength of disorder and different ranges with fraction of broken fibers $(1-U)$ in one dimension.
1d model: It can be seen from the left panel that for both high range and high $\beta$ values, the curves merge with the inverted parabola $U(1-U)$ expected for completely random failures.
2d model: In 2d model the reference for random fractuaring is set by the two dimensional random site percolation problem. Our results are then compared with it.

situations are different. For two dimensions the situation is qualitatively similar. But the general shape of the curve for random failure is not known. However, there are many numerical studies in terms of random site percolation (see Ref. [112] and references therein) that looks at density of patches under random occupations.

### Compression of areas under $n_p$ v/s $U$ for different ranges

We already know that, for random failure process on a 1d chain the probability of having a patch will be given by $U(1-U)$. So, the area under the $n_p$ v/s $1-U$ for such uncorrelated failure is:

$$A = \int_0^1 U(1-U)dU = 1/6 \tag{5.1}$$

Any daviation of area from this above mentioned value will signify correlated and nucleating failure. Here we study the area $A$ under the $n_p$ v/s $U$ curves. Area $A$ becomes independent of $R$ and approaches $1/6$ as we go to higher range value. In

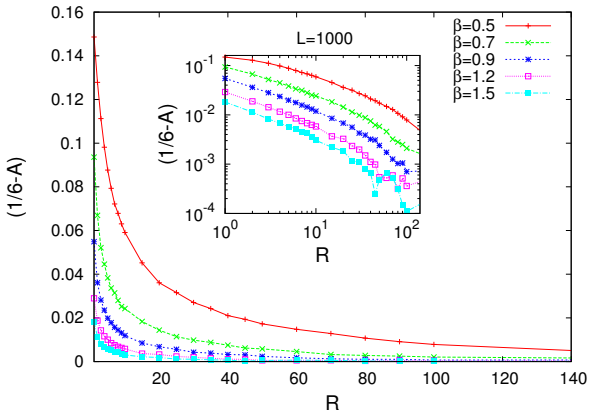


Figure 5.3: Area under the $n_p$ v/s $1-U$ curve is shown with a continuous variation of $R$ for different disorder $\beta$ within 0.5 and 1.5. As $\beta$ increases the area approaches 1/6. Although at high $R$ since the fracture is already random the effect of $\beta$ is not evident.

this limit we can say the mean-field regime is reached. This measure again gives a crossover scale $R_c$. At a particular $\beta$ value we increase the range $R$ and keep observing the area under $n_p$ v/s $1-U$ curve. At a particular $\beta$, $R_c$ is the range value for which $(1/6 - A) < 10^{-3}$.

### 5.3.2 Boundary between abrupt and non-abrupt failure

The regions with abrupt or brittle like failure ($B$ and $D$) and non-abrupt or quasi-brittle like failure ($A$ and $C$) can be separated by noting but the fraction of surviving fiber $U_c$ just before the global failure. When $U_c = 1$, the failure is abrupt as the breaking of the first fiber leads to complete breakdown of the system. When $U_c < 1$, the failure is no longer abrupt. We keep the $R$ fix (for $R > R_c$ or $R < R_c$) and set the disorder at a low value. This gives $U_c = 1$. Now if we increase the disorder slowly then a point on the boundary is constructed by such a disorder value above which $U_c < 1$. Repeating this study for different $R$ values we obtain a boundary that separates both nucleating and percolating failure region into two parts each: brittle and quasi-brittle.

Now, part of this line in the region $R > R_c$, that separates region $D$ from region

$C$, does not depend on system size, since it is in the mean-field regime (note that non-abrupt failure occurs much before complete uncorrelated failure in the large $\beta$ region). A transition from brittle to quasi-brittle region occurs across this part of the boundary [100, 114] (See chapter 3 subsection 3.1.1).

The part of the boundary in the region $R < R_c$, separating region $B$ from region $A$, is system size dependent. This line moves to higher value as we go to higher system size (See chapter 2 subsection 3.1.2), increasing the amount of brittle region.

### 5.3.3 Boundary of high disorder regime

One of the universal behavior that fiber bundle model shows in quasi-brittle mean field limit is the scale free distribution for avalanche with an unique exponent value $-5/2$. This falls in the region $C$ of the phase diagram. By keep increasing disorder value we can reach the high disorder limit (region $E$). At very high disorder the threshold of the fibers are very distinct from each other. So, hardly any avalanches

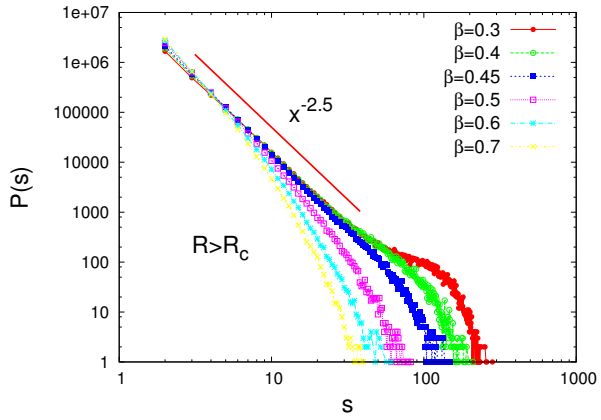


Figure 5.4: Avalanche size distribution in the region $R > R_c$ for disorder ranging from 0.3 to 0.7. As the disorder value crosses 0.5, the avalanche size distribution deviates from the scale free behavior (with exponent $-5/2$). A set of such $(R, \beta)$ values above which this deviation takes place, gives us the boundary of high disorder.

takes place in this region. For $R > R_c$, we have started from a disorder value in region $C$ and keep increasing. The boundary is formed by all those disorder values

beyond which the model deviates from the universal scale free nature of avalanche distribution.

Another way of looking into this boundary is studying the scaling of $R_c$ with system size. As discussed in chapter 4, we find $R_c \sim L^{1-\alpha}$, where $\alpha$ has a constant value 1/3 in quasi-brittle (intermediate disorder) region. As shown in figure 5.5, $R_c \sim L^{2/3}$ up to $\beta = 0.5$. Beyond this disorder as the model entries the high

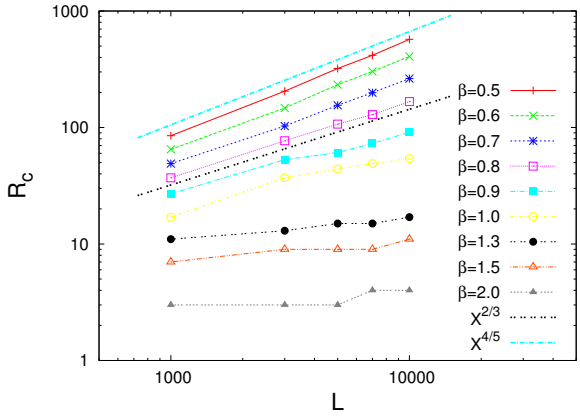


Figure 5.5: Scaling of $R_c$ with system size is observed at different disorder values. As we cross the boundary of high disorder region, the scaling deviates from $L^{2/3}$ (see chapter 4). At very high disorder $R_c$ comes to a very low value and becomes independent of $L$.

disorder region, the exponent changes towards zero value and gradually $R_c$ becomes independent of system size. In this high disorder limit the failure process is always random ($R_c$ is very small) irrespective of range as well as system size is.

## 5.4 Conclusion

Using the criteria outlined above, we arrive at the quantitative phase diagram for fiber bundle model in one and two dimensions (see Fig. 5.1). Almost all the studies in fiber bundle model fall in some point of this phase diagram. The most studied region being the region $C$, which is also historically the earliest. Subsequently region $A$ was studied, which is qualitatively different from region $C$ in the sense that we

no longer observe scale free avalanche statistics here. The region $B$ and $D$ shows abrupt failure and thus experimentally not that accessible. This two regions ($B$ and $D$) are only separated in terms of spatial correlation of rupture events. Finally we come to region $E$ at high disorder limit where hardly any precursory activity is seen. The failure process in this region can be compared with random percolation events. In conclusion, we provide a framework in fiber bundle model to incorporate previous studies of different phases and the crossovers and transitions between them by providing a scaling criterion.

# Chapter 6

# Discussions on the thesis work

We have seen that disorder and stress release range have their effects in fracture process in statistical mechanical models namely fiber bundle model and spring ladder model. Disorder is introduced in these models as fluctuation of local strength of individual elements. In fiber bundle model range is defined as number of fibers that carries the load due to rupture process. In spring ladder model the angular spring constant takes care of the range in the model.

In mean field limit (equal load sharing scheme) at low disorder ($\delta$) the failure process is abrupt like brittle materials and does not show any plastic region in the response curve. With increasing $\delta$ value we get a critical disorder $\delta_c$ around which the model shows a brittle to quasi-brittle like transition. Above this critical disorder the model shows precursory events during failure process. Critical behavior of $\delta_c$ is studied through the divergence of relaxation time and scale free behavior of avalanche size distribution. In local load sharing case the system size ($L$) effect comes into the play and the strength $\sigma_c$ decreases with increase in $L$. At high disorder $\sigma_c \sim 1/\log L$. on the other hand at low disorder $\sigma_c \sim 1/L$, following the weakest link of the chain algorithm. We characterize a disorder window within which this change from scale free behavior to inverse logarithmic behavior occurs.

Change in stress release range changes the rupture pattern during the failure process. In fiber bundle model we have shown that increase in stress release range makes the rupture pattern of individual elements uncorrelated. There is a critical range value $R_c$ around which the spatial correlation vanishes. $R_c \sim L^{1-\alpha}$. For $\delta > \delta_c$, $\alpha = 1/3$ and our findings matches with the literature. For $\delta < \delta_c$, $\alpha$ is an increasing function of $\delta$ and above scaling exponent changes with disorder. In spring ladder model, the range is controlled through the angular force constant $k_\alpha$. With increasing $k_\alpha$ value, the correlation in rupture process vanishes gradually.

Now if we tune both the disorder ($\beta$, in case of power law redistribution) and range ($R$), it is expected to get failure process which will be combinations of abrupt/non-abrupt and correlated/random failure. By tuning both range $R$ and disorder $\delta$, we have shown all 5 regions that can be found for fiber bundle model on $R - \beta$ plane. In different regions we get the following failure processes: (a) brittle nucleating (correlated and abrupt failure), (b) quasi-brittle nucleating (correlated but non-abrupt failure), (c) brittle percolating (random and abrupt failure), (d) quasi-brittle percolating (random and non-abrupt failure), (e) high disorder limit (failure without showing avalanches).

As an outcome of the thesis, we have worked mainly in fiber bundle model with varying disorder and stress release range, characterizing different regions with unique failure process. A tensorial approach through spring ladder network is also performed with varying angular force constant, which is the key parameter to control the stress release range. We have characterized different modes of fracture development (brittle or quasi-brittle fracture, avalanche dynamics etc.) and fracture morphology (nucleating or percolating) for different values of disorder strength $\delta$ (or $\beta$) and stress release range $R$ in fiber bundle model. We have compared our results with the known observations in random resistor network and random spring network.

# List of Figures

1.1 Variation of cohesive stress with increasing separation between atoms. $a_0$ is the inter atomic spacing at unstrained condition. . . . . 22

1.2 Motion of a dislocation through crystal plane is shown in the figure. This motion leads to slip in between the planes. . . . . 24

1.3 Notch effect in real system is shown in the figure. The stress at the edges of the crack is much higher than the external stress,0 depending on the major (c) and minor axes (b) of the elliptical crack. . . . . 24

1.4 Above figures shows the failure probability, $F(\sigma)$, of materials at low disorder limit (Eq.1.12, left figure) and intermediate disorder limit (Eq.1.13, right figure). In both limits, $F(\sigma)$ increase as we go to higher stress values. The rate of this increase is faster for higher volume $V$. . . . . 27

1.5 Left: Experimental set up for acoustic emission experiment. A number of acoustic sensors are attached to the material. The energy release in fracture process is recorded through these sensors. Right: AE signals collected through the sensors. Energy emitted in failure process is plotted against the applied stress value. The density of signal is very high near the failure point. . . . . 30

1.6 Response curve of brittle, quasi-brittle and ductile materials. Brittle materials show perfectly linear response prior to an abrupt failure. Both quasi-brittle and ductile materials have appreciable plastic region. Only difference is ductile materials show permanent deformation even when the applied stress is withdrawn. . . . . 32

1.7 The figure shows brittle to ductile transition with varying temperature. The energy release in fracture process falls very rapidly around a critical temperature $T_c$ which is the brittle to ductile transition point. 34

1.8 Fracture process zone (FPZ) near the crack tip for brittle and plastic failure is shown. Brittle cracks hardly shows any FPZ while one the other hand in case of plastic failure we get certain amount of FPZ within which the energy due to fracture process is stored. . . . . 36

2.1 A two dimensional spring network model is shown, at both unstrained condition (left) and with a spring broken due to the application of external force (right). . . . . 38

2.2 Left: 2d inverted square lattice shaped random resistor network. A potential deference $V$ is applied to the model creating a current flow $I$. Right: A particular mess of involving five lattice point is observed to explain the breaking criterion and redistribution. . . . . 40

2.3 Fiber Bundle Model : Hookean fibers with random thresholds attached between two parallel bars. The figure shows the behavior of the bars in case of equal load sharing (ELS) and local load sharing (LLS) scheme. . . . . 43

3.1 Fraction of unbroken bonds $U^*$ is plotted for different $\sigma_{ext}$ and $\delta$. In yellow region $U^* = 1$, while in the black region $U^* = 0$. The color gradient corresponds to partially broken configurations ($0 < U^* < 1$). At low $\delta$ values, the system goes from yellow to black region at a critical stress with an abrupt fracture. For $\delta > \delta_c$, the system goes from yellow to black region through a color gradient region signifying gradual fracture at different stress levels. The boundary of black region gives us the critical stress $\sigma_c$ for the system. . . . . 50

3.2 Plot of $P_b$ with $\delta$ for increasing system size values $L = 100$(star), 500(square), 1000(open circles), 5000(filled circles) and $10,000$(tringle). For low $\delta$, $P_b$ is close to 1. As $\delta$ increases, $P_b$ decreases till it goes to zero. This fall becomes more and more sharper as the system size is increased. In the inset variation of $P_b$ with system size $L$ is shown for $\delta = 0.15$(star), 0.1666(square) and 0.18(open circle). For $\delta = 0.15$, $P_b$ saturates, so that there is always a non-zero $P_b$ value. For $\delta = 0.18$, $P_b$ falls to zero exponentially fast. At $\delta_c$, $P_b \sim L^{-\eta}$, with exponent $\eta \approx 1/3$. . . . . 51

3.3 Relaxation time $\tau$ is plotted with $\delta$ for system sizes $L = 10000$(star), 30000(square), 50000(hollow circle), 70000(filled circle) and 100000(triangle). In the inset the scaling of $\tau$ is shown. The scaling is done by plotting $\tau L^{-\beta}$ against $(\delta - \delta_c)L^{1/\nu}$ for the above mentioned $L$ values with $\beta = 0.33 \pm 0.02$. . . . . 52

3.4 $P(s)$ vs. $s$ is plotted for $\delta = 0.15$(star), 0.1666(square) and 0.18(filled circle). For $\delta < \delta_c$, the distribution levels off. Since in this region the avalanches are uncorrelated there is always a probability of having an avalanche of any size (even as big as the system size). For $\delta > \delta_c$, $P(s)$ falls to zero exponentially fast and there is no big avalanches found. At $\delta = \delta_c$, $P(s)$ falls in a power law behavior with exponent $\kappa = 0.5 \pm 0.01$. . . . . 54

3.5 (a) Variation of brittle and quasi-brittle region with system size ($L$) for the most local load sharing scheme. Brittle region increases with increasing system size.
(b) System size independent brittle and quasi-brittle region in mean field case. The division of the regions happens around $\delta_c = 1/6$. . . . 55

3.6 $L^*$ is the system size above which the fracture is purely abrupt. Variation of $L^*$ with disorder for LLS scheme. Below $\delta = \delta^*$ the fracture is always abrupt and its really easy to achieve . This is the pure brittle region. For $\delta > \delta^*$ there is a certain region below $L^*$ where the failure is quasi-brittle like non abrupt. . . . . 56

3.7 Left figure: Study of $\sigma_c$ with continuous variation of disorder value ($\delta$). Results are generated for system sizes ranging from $10^3$ to $5\times10^4$. Dotted line gives the yield stress ($\sigma_y$), the separation of elastic and plastic region. $\delta_L$ is the disorder below which we get brittle failure. $\delta_L$ increases with increasing $L$ values. Right figure: $U_c$ is studied with LLS scheme for different system sizes ($10^3 \geq L \geq 5 \times 10^4$) with increasing $\delta$ values. The value of $\delta_L$ below which $U_c = 1$ is the disorder value separating brittle region from the quasi-brittle one. Increase in system size shows increase in $U_c$ value and hence leads the model to higher abruptness. . . . . 58

3.8 Lower: $\sigma_c - \sigma_l$ is plotted against $1/\log L$ at different $\delta$ values. Clearly the data gives a straight line for higher disorder ($0.4 < \delta < 0.5$) and at that region the logarithmic behavior matches with numerical data with less error. At low disorder it deviates from the line.
Upper: $\sigma_c - \sigma_l$ is plotted against $L$ in log scale. For low disorder it shows a scale free behavior with slope $-1$. Above $\delta = 0.35$ this slope changes rapidly and saturates to very low value ($\approx 0.2$) and the system size effect becomes very weak. Here the logarithmic behavior is more appropriate. . . . . 60

3.9 Numerical data for system size effect of critical stress is fitted with $f(x) = p + qL^{-r}$ (power law behavior) and $g(x) = a + b/\log L$ (logarithmic behavior). The fitting is done for $\delta = 0.1$, 0.2, 0.3, 0.35, 0.4 and 0.5. For high disorder ($\delta > 0.4$) value both $f(x)$ and $g(x)$ matches with the data with less error. At low disorder ($\delta < 0.3$) the power law behavior matches much accurately than the logarithmic one. 61

3.10 The exponents from figure 3.8 ($r$ and $b$) are shown with a continuous variation of disorder. Both $r$ and $b$ remains at a same value for $\delta > 0.4$ as well as $\delta < 0.3$. Within the region $0.3 < \delta < 0.4$ these exponents shows abrupt changes. This is the transition region where the simulated data shifts from power law to logarithmic behavior. . . 61

3.11 Study of $U(t, \sigma_c, \delta)$ with increasing time steps for system sizes $10^5$, $2 \times 10^5$ and $3 \times 10^5$. Disorder is kept fixed at $\delta = 0.1$. The black dotted lines show the analytical behavior according to Eq. 3.16 with $\epsilon = 0.0025$, $\epsilon = 0.0015$ and $\epsilon = 0.0008$ respectively. The envelop of the curve increases as well as $\epsilon$ decreases as we go to higher system sizes. . . . . 63

3.12 The distribution for failure time for different $\delta$ is fitted with Weibull distribution with shape parameter $k$ and scale parameter $\lambda$. The numerical results are fitted with various $k$ and $\lambda$ values. In the inset the variation of shape parameter $k$ is shown with $\delta$. . . . . 64

3.13 System size effect of maximum average relaxation time $\tau_f$ at different $\delta$ value. $\tau_f$ shows a scale free behavior with system size ($L$) : $\tau_f \sim L^{\alpha}$. Value of exponent $\alpha$ remains constant at 1/3 for $\delta > \delta_c$, while it keeps decreasing below $\delta_c$ and the system size effect of $\tau_f$ gradually vanishes. Inset: Variation of scaling exponent $\alpha$ with varying disorder value. For $\delta > \delta_c$, $\alpha$ saturates at a value 1/3. Below $\delta_c$ the exponent value decreases as we go to lower $\delta$ values. . . . . 65

4.1 The upper panel shows the variation of the stresses on the fibers in the system with redistribution steps $\tau$. The onset of nucleation can be seen from the tip of the cone, beyond which one broken patch grows and the total number of patch starts decreasing. The onset time gets shifted to a higher value as the stress redistribution range $R$ is increased ((a)-(c)) and expected to merge with failure time in the global load sharing limit. The panel below ((d)-(f)) shows the variation of average stress per fiber ($\langle\sigma\rangle$; denoted by dotted lines) and number ($n_p$) of patches (denoted by solid lines), scaled by system size, for corresponding $R$ values. The onset of nucleation ($\tau_n$) is the point where the number of patch starts decreasing and the stress per fiber saturates (at the critical value) until failure point ($\tau_f$) is reached. 70

4.2 The data collapse for the time difference $\Delta\tau = \tau_f - \tau_n$ for different system sizes $L$ and for different range $R$ as given by the scaling form Eq. (4.1). The inverse decay marks the nucleation regime, which stops when $R \sim L^{2/3}$ and global load sharing region begins. In this regime, $\Delta\tau$ becomes $R$ independent but depends on $L$ (as can be seen from the inset). The initial collapsed region in the inset confirms the dependence $\Delta\tau \sim L/R$ in the nucleation regime, and the lines spreads out as soon as global mode starts dominating. . . . . 73

4.3 The top figure (a) shows the variation of the onset time for nucleation $\tau_n$ and failure time $\tau_f$ with system size $L$ for two values of $R$. For small system sizes and bigger $R$ value, the two times are very close to each other. In this region, mean-field 'critical behavior' can be observed. For fixed $R$ value, this 'criticality' will not survive in the large system size limit. The figure at the bottom (b) shows the avalanche size distribution for fixed $R$ value (100) while the system size is increased. For $L = 10^3$, the ratio $R/L^{2/3} = 1$, putting the system in the critical regime where $P(S) \sim S^{-2.5}$. But for $L = 10^4$ and $L = 10^5$ the ratio becomes $\approx 0.215$ and $\approx 0.046$ respectively. The avalanche size distribution in the last two cases deviates from the above scale free distribution. . . . . 74

4.4 The left figure (a) shows that the failure threshold $\sigma_c$ goes to zero with $1/\ln L$ when $\gamma < \gamma_c = 4/3$ in the case of power-law load redistribution, showing the validity of the proposed scaling criterion that the effective range must scale faster than $L^{2/3}$ (or $\gamma < 4/3$) for global load sharing mode. The inverse logarithmic decay is similar to what is observed for uniform load sharing within range $R$ for $R < L^{2/3} < 1$ (b). . . . . 75

4.5 The spring ladder model with external force $F$ applied on the lower layer nodes (a) before breaking of a spring and (b) after breaking of a spring showing the deformed network. . . . . 77

4.6 Variation of fraction of unbroken springs,just before the global failure, with $k_\alpha$ values for system sizes $10^3$, $5 \times 10^3$ and $10^4$. For low $k_\alpha$, $U_c$ is quite high and the failure process is abrupt. At high $k_\alpha$ values the result matches with the existing results of ELS fiber bundle model. . 80

4.7 The number of clusters per site is plotted with increasing fraction of broken springs $(1 - U)$, for $k_\alpha$ values $10^{-3}$, 10 and $10^4$. The behavior is compared with the random fratuaring event on a 1d chain. . . . . 81

4.8 The avalanche size distribution at different $k_\alpha$ values. The exponent of the power law behavior is seen shifting from the ELS value of 2.5 to a LLS value of 4.8 as $k_\alpha$ decreases. . . . . 82

5.1 The figure shows all the regions on $R - \beta$ plane for 1d chain and 2d bundle. $B$ and $D$ are brittle region and shows abrupt failure. $A$ and $C$ shows quasi-brittle response. In region $A$ and $B$ the rupture process is correlated. In region $E$, there are no avalanches and the fracture process is percolation like random. . . . . 86

5.2 The variations of density of patch $n_p$ are shown for (a-c) constant range and different strength of disorder ($\beta$) and for (d-f) constant strength of disorder and different ranges with fraction of broken fibers $(1-U)$ in one dimension. 1d model: It can be seen from the left panel that for both high range and high $\beta$ values, the curves merge with the inverted parabola $U(1-U)$ expected for completely random failures. 2d model: In 2d model the reference for random fractuaring is set by the two dimensional random site percolation problem. Our results are then compared with it. . . . . 89

5.3 Area under the $n_p$ v/s $1-U$ curve is shown with a continuous variation of $R$ for different disorder $\beta$ within 0.5 and 1.5. As $\beta$ increases the area approaches 1/6. Although at high $R$ since the fracture is already random the effect of $\beta$ is not evident. . . . . 90

5.4 Avalanche size distribution in the region $R > R_c$ for disorder ranging from 0.3 to 0.7. As the disorder value crosses 0.5, the avalanche size distribution deviates from the scale free behavior (with exponent $-5/2$). A set of such $(R, \beta)$ values above which this deviation takes place, gives us the boundary of high disorder. . . . . 91

5.5 Scaling of $R_c$ with system size is observed at different disorder values. As we cross the boundary of high disorder region, the scaling deviates from $L^{2/3}$ (see chapter 4). At very high disorder $R_c$ comes to a very low value and becomes independent of $L$. . . . . 92

# Bibliography


[1] *Mechanical metallurgy*, G. E. Dieter, New York, McGraw-Hill (1993).

[2] *Statistical Phtsics of Fracture and Breakdown in Disordered Systems*, B. K. Chakrabarti and L. G. Benguigui ,Oxford Univ. Press, Oxford (1997).

[3] *Statistical Models for the Fracture of Disordered Media*, Eds H. Herrmann and S. Roux, North-Holland, Amsterdam (1990).

[4] *Fracture of Brittle Solids*, B. R. Lawn, Cambridge University Press, Cambridge (1995).

[5] F. Appel, H. Bethge and U. Messerschmidt, phys. stat. sol. (a) **42**, 6171 (1977).

[6] M. Wollgarten, M. Beyss, K. Urban, H. Liebertz and U. Kster, Phys. Rev. Lett. **71**, 549 (1993).

[7] C. E. Inglis, Trans. Inst. Naval Architects, vol **55**, pt. I, pp. 219-230 (1913).

[8] E. Orowan, Welding J., vol **34**, 157s-160s (1955).

[9] A. A. Griffith, Phil. Trans. Roy. Soc. London, vol. **221A** (1920), pp. 163-198; First Intn. Congr. Appl. Mech., Delft, p. 55 (1924).

[10] *Griffith Criterion for Glass Fracture*, O. L. Anderson, John Wiley and Sons Inc., Newyork, pp. 331-353 (1959).

[11] F. Otto, J. Am. Ceramic Soc, vol **38**, p. 123 (1955).

[12] S. S. Brenner, J. Appl. Phys., vol. **27**, p. 1484 (1956).

[13] P. Ray and B. K. Chakrabarti, Solid State Commun., **53**, 477 (1985).

[14] M.Tanaka, R.Kato, and A.Kayama, Journal of materials science **37**, 3945-3951 (2002).

[15] F. A. McClintock, *Statistics of Brittle Fracture, in The Fracture Mechanics of Ceramics*, edited by Bradt R. C. et al., Vol. I (Springer-Verlag, US), p. 93 (1974).

[16] Z. P. Bazant, Probabilistic Engineering Mechanics **19**, 307-319 (2004).

[17] J. P. Dempsey, R. M. Adamson and S. V. Mulmule, Int. J. Fract. **95** (1999),

[18] Marcel R.A. van Vliet and Jan G.M. van Mier, Engineering Fracture Mechanics **65**, Issues 23, 165188 (2000).

[19] Z. P. Bazant and P. A. Pfeiffer, ACI Mater. J. **84**, 463480 (1987).

[20] Z. P. Bazant and Z. Li, J. Struct. Eng. **121**, 739746 (1995).

[21] I. C. van den Born, A. Santen, H. D. Hoekstra and J. Th. M. De Hosson, Phys. Rev. B **43**, 3794(R) (1991).

[22] *Heterogeneous Materials II: Nonlinear and Breakdown Properties*, M. Sahimi, Springer-Verlag, New York (2003).

[23] Z. P. Bazant, PNAS **101**, 13400 (2004).

[24] P. M. Duxbury and P. L. Leath, J. Phys. **A20**, L411 (1987).

[25] *Fracture and size effect in concrete and other quasi-brittle material*, Z. P. Bazant, CRC Press LLC (1998).

[26] M. J. Alava, P. K. V. V. Nakula and S. Zapperi, J. Phys. D **42**, 214012 (2009b).

[27] C. Lu, D. V. Jones and H. Takayasu Phys. Rev. Lett. **82**, 347 (1999).

[28] A. Petri, G. Paparo, A. Vespignani, A. Alippi, and M. Costantini, Phys. Rev. Lett. **73**, 3423 (1994).

[29] S. Zapperi, A. Vespignani and H. E. Stanley, Nature **388**, 658 (1997b).

[30] J. P. Sethna, K. A. Dahmen and C. R. Myers, Nature **410**, 242 (2001).

[31] A. Guarino, S. Ciliberto, A. Garcimartin, M. Zei, and R. Scorretti, Eur. Phys. J. B **26**, 141-151 (2002).

[32] A. Garcimartin, A. Guarino, L. Bellon, and S. Ciliberto, Phys. Rev. Lett. **79**, 3202 (1997).

[33] C. Maes, A. Van Moffaert, H. Frederix, and H. Strauven, Phys. Rev. B **57**, 4987 (1998).

[34] S. Pradhan, A.M. Stroisz, E. Fjr, J. Stenebrten, H. K. Lund, E. F. Snsteb and S. Roy, ARMA **14-7442** (2014), arXiv:**1512.05184**, (2015).

[35] *Essentials of Materials Science and Engineering*, D. R. Askeland and W. J. Wright, SI Edition (2008).

[36] *The Brittle-Ductile Transition in Rocks*, A. G. Duba, W. B. Durham, J. W. Handin and H. F. Wang, Geophysical Monograph Series (2013).

[37] T. Wonga and P. Baudb, Journal of Structural Geology, vol **44**, 25-53 (2012).

[38] M. Brede and P. Haasen, Acta Metallurgica, Volume **36**, Issue 8, pp. 2003-2018 (1988).

[39] P. Gumbsch, J. Riedle, A. Hartmaier, H. F. Fischmeister, Science, Vol. **282**, Issue 5392, pp. 1293-1295 (1998).

[40] R. Li, K. Sieradzki, Phys. Rev. Lett. **68**, 1168 (1992).

[41] J. R. Rice and R. Thomson, Philos. Mag. **29**, 73 (1974).

[42] G. Schocek, Philos. Mag. A **63**, 111 (1991).

[43] J. R. Rice, J. Mech. Phys. Sol. **40**, 239 (1992).

[44] P. B. Hirsch, S. G. Roberts and J. Samuels, Proc. R. Soc. Lond. A **421**, 25 (1989).

[45] W.W. Oerbcrich, H. Huang, W. Zielinski and P. G. Marsh, Metall. Trans. A **24A**, 535 (1993).

[46] M. Khantha, D.P. Pope, V. Vitek, Materials Science and Engineering A **234-236**, 629-632 (1997).

[47] M. Khantha, D.P. Pope, V. Vitek, Scripta Metallurgica et Materialia, Vol. **31**, No. 10, pp. 1349-1354 (1994).

[48] C. B. Picallo, J. M. Lopez, S. Zapperi and M. J. Alava, Phys. Rev. Lett. **105**, 155502 (2010).

[49] J. S. Langer and Alexander E. Lobkovsky, Phys. Rev. E **60** (1999), 6978.

[50] J. Scheibert, C. Guerra, F. Clari, D. Dalmas, and D. Bonamy, Phys. Rev. Lett. **104**, 045501 (2010).

[51] D. Vere-Jones, Journal of the International Association for Mathematical Geology, **9**, 455-481 (1977).

[52] K. S. Chana, P. Jonesb and Q. Wangb, Materials Science and Engineering: A **341**, 18-34 (2003).

[53] X. Z. Hu, F. H. Wittmann, Materials and Structures **25**, 319-326 (1992).

[54] Z.P. Bazant and M.T. Kazemi, International Journal of Fracture **44**, 111-131 (1990).

[55] W. A. Curtin, Phys. Rev. Lett. **80**, 1445 (1998).

[56] W. A. Curtin and H. Scher, Phys. Rev. Lett. **67**, 2457 (1993).

[57] P. K. V. V. Nukula, S. imunovi, S. Zapperi, J. Stat. Mech **2004**, P08001 (2004).

[58] B. Kahng, G. G. Batrouni, S. Redner, L. de Arcangelis, H. J. Herrmann, Phys. Rev. B **37**, 7625 (1988).

[59] A. Shekhawat, S. Zapperi, J. P. Sethna, Phys. Rev. Lett. **110**, 185505 (2013).

[60] A. A. Moreira, C. L. N. Oliveira, A. Hansen, N. A. M. Araujo, H. J. Herrmann, J. S. Andrade, Jr., Phys. Rev. Lett. **109**, 255701 (2012).

[61] H. A. Knudsen and Sandor Fazekas, J. Comp. Phys **211**, 700-718 (2008).

[62] K. Wu and R. M. Bradley, Phys. Rev. E **49**, 1712 (1994).

[63] G. G. Batrouni, A. Hansen and J. Schmittbuhl, Phys. Rev E **65**, 036126 (2002).

[64] S. Pradhan, A. Hansen, and B. K. Chakrabarti, Rev. Mod. Phys. **82**, 499 (2010).

[65] A. Hansen, P. C. Hemmer & S. Pradhan, *The Fiber Bundle Model: Modeling Failure in Materials* Wiley VCH Berlin (2015).

[66] F. T. Pierce, J. Text. Ind. **17**, 355 (1926).

[67] H. E. Daniels and T. H. R. Skyrme, Adv. Appl. Probab. **21**, 315 (1989).

[68] S. L. Phoenix, Adv. Appl. Probab. **11**, 153 (1979).

[69] R. L. Smith and S. L. Phoenix, J. Appl. Mech. **48**, 75 (1981).

[70] W. I. Newman and S. L. Phoenix, Phys. Rev. E **63**, 021507 (2001).

[71] D. G. Harlow and S. L. Phoenix, J. Compos. Mater. **12**, 314 (1978).

[72] D. G. Harlow and S. L. Phoenix, Adv. Appl. probab. **14**, 68 (1982).

[73] R. L. Smith, Proc. R. Soc. London, Ser. A **382**, 179 (1982).

[74] S. Pradhan, B. K. Chakrabarti, and A. Hansen, Phys. Rev. E **71**, 036149 (2005).

[75] R. C. Hidalgo, Y. Moreno, F. Kun, and H. J. Herrmann, Phys. Rev. E **65**, 046148 (2002).

[76] S. Biswas, S. Roy and P. Ray, Phys. Rev. E, **91**, 050105(R) (2015).

[77] S. Pradhan and A. Hansen, Phys. Rev. E **72**, 026111 (2005).

[78] J. V. Andersen, D. Sornette, and K. T. Leung, Phys. Rev. Lett. **78**, 2140 (1997).

[79] S. Pradhan, P. Bhattacharyya, and B. K. Chakrabarti, Phys. Rev. E **66**, 016116 (2002).

[80] C. Roy, S. Kundu, and S. S. Manna, Phys. Rev. E **87**, 062137 (2013).

[81] A. Stormo, K. S. Gjerden and A. Hansen, Phys. Rev. E **86**, 025101(R) (2013).

[82] S. Pradhan and P. C. Hemmer, Phys. Rev. E **75**, 056112 (2007).

[83] Z. P. Bazant, S. D. Pang, M. Vorechovsky, D. Novak, R. Pulk, Fracture Mechanics of Concrete Structures, Li et al (eds) Ia-FraMCos, **ISBN 0 87031 135 2**, (2004).

[84] S. G. Bardenhagen, J. U. Brackbill and D. Sulsky, Phys. Rev.E **62**, 3 (2000)

[85] Alberto Carpinteri, Int. J. Solids Structures **31**, No. 3, 291-302 (1994).

[86] Hansen, A. and P. C. Hemmer, Trends in Stat. Phys **1**, 213 (1994).

[87] S. D. Zhang and E. J. Ding, Phys. Lett. A **193**, 425 (1994).

[88] M. Kloster, A. Hansen, and P. C. Hemmer, Phys. Rev. E **56**, 2615 (1997).

[89] S. D. Zhang and E. J. Ding, J. Phys. A **28**, 4323 (1995).

[90] S. D. Zhang, E. J. Ding, Phys. Rev. B **53**, 646 (1996).

[91] D. G. Harlow and S. L. Phoenix, J. Mech. Phys. Solids **39**, 173 (1991).

[92] Pradhan, S. and B. K. Chakrabarti, Int. J. Mod. Phys. B **17**, 5565 (2003a).

[93] W. Weibull, J. Appl. Mech., **18** (2), pp. 293297 (1951).

[94] R. Danzer, P. Supancic, J. Pascual, T. Lube, Engineering Fracture Mechanics **74**, 29192932 (2007).

[95] B. Basua, D. Tiwari, D. Kunduc, R. Prasada, Ceramics International **35**, 237246 (2009).

[96] R. Danzer, Journal of the European Ceramic Society **10**, 461-472 (1992).

[97] C. Lu, R. Danzer and F. D. Fischer, Phys. Rev. E **65**, 067102 (2002).

[98] W. A. Curtin, M. Pamel, and H. Scher Phys. Rev. B **55**, 12051 (1997).

[99] W. A. Curtin and H. Scher, Phys. Rev. B **55**, 12038 (1997).

[100] S. Roy and P. Ray, EPL, **112**, 26004 (2015).

[101] A. Shekhawat, S. Zapperi, J. P. Sethna, Phys. Rev. Lett. **110**, 185505 (2013).

[102] M. J. Alava, P. K. V. V. Nukala, S. Zapperi, Adv. Phys. **55**, 349 (2006).

[103] A. A. Moreira, C. L. N. Oliveira, A. Hansen, N. A. M. Araújo, H. J. Herrmann, J. S. Andrade, Jr. Phys. Rev. Lett. **109**, 255701 (2012).

[104] J. Baró, Á. Corral, X. Illa, A. Planes, E. K. H. Salje, W. Schranz, D. E. Soto-Parra, E. Vives, Phys. Rev. Lett. **110**, 088702 (2013).

[105] R. C. Hidalgo, Y. Moreno, F. Kun, H. J. Herrmann, Phys. Rev. E **65**, 046148 (2002).

[106] D. G. Harlow, S. L. Phoenix, J. Composite Mater. **12**, 195 (1978).

[107] S. Pradhan, B. K. Chakrabarti, A. Hansen, Phys. Rev. E **71**, 036149 (2005).

[108] A. Stormo, K. S. Gjerden, A. Hansen, Phys. Rev. E **86**, 025101(R) (2012).

[109] S. Biswas, B. K. Chakrabarti, Eur. Phys. J. B **86**, 160 (2013).

[110] F. Kun, S. Zapperi, H. J. Herrmann, Eur. Phys. J. B **17**, 269 (2000).

[111] H. E. Daniels and T. H. R. Skyrme, Adv. Appl. Probab. **21**, 315 (1989).

[112] R. M. Ziff, S. R. Finch, V. S. Adamchik, Phys. Rev. Lett. **79**, 3447 (1997).

[113] S. Roy, S. Biswas and P.Ray, arXiv:**1606.06062** (2016).

[114] C. Roy, S. Kundu, S. S. Manna, Phys. Rev. E **91**, 032103 (2015).